# CARBON DIOXIDE EMISSIONS BY ROCK ORGANIC CARBON OXIDATION AND THE NET GEOCHEMICAL CARBON BUDGET OF THE MACKENZIE RIVER BASIN

KATE HORAN*,†, ROBERT G. HILTON**, MATHIEU DELLINGER**,
ED TIPPER***, VALIER GALY§, DAMIEN CALMELS§§, DAVID SELBY*,
JÉRÔME GAILLARDET§§§, CHRIS J. OTTLEY*, DANIEL R. PARSONS‡, and
KEVIN W. BURTON*

ABSTRACT.    The exposure of organic carbon in rocks to oxidative weathering can release carbon dioxide ($CO_2$) to the atmosphere and consume atmospheric oxygen. Alongside volcanism, metamorphism, and the weathering of carbonate minerals by sulfuric acid, this is a major source of atmospheric $CO_2$ over million year timescales. The balance between $CO_2$ release and $CO_2$ drawdown by silicate weathering and organic carbon burial sets the net geochemical carbon budget during weathering and erosion. However, the rates of rock-derived organic carbon (petrogenic organic carbon, $OC_{petro}$) oxidation remain poorly constrained. Here, we use rhenium as a proxy to trace and quantify $CO_2$ release by $OC_{petro}$ oxidation in the Mackenzie River Basin, Canada, where the other carbon fluxes have been well constrained previously. River water and sediment samples were collected between 2009 and 2013 at gauging stations along the Mackenzie River and its main tributaries (Liard, Peel and Arctic Red). To assess rhenium inputs from silicate, sulfide and $OC_{petro}$ mineral phases we normalize dissolved rhenium concentrations, $[Re]_{diss}$, to sodium and sulfate ion concentrations. This approach suggests that >85 percent of $[Re]_{diss}$ is derived from $OC_{petro}$ in the main river channels. $[Re]_{diss}$ and water discharge measurements are used to quantify dissolved Re yields. River sediments provide a measure of the Re to $OC_{petro}$ ratio of materials undergoing weathering in the basin, and agree well with published rock samples. Dissolved Re yields are combined with river sediment $[Re]/[OC_{petro}]$ ratios to estimate the $CO_2$ emissions by $OC_{petro}$ weathering. These are $0.45\,^{+0.19}/_{-0.11}$ metric tonnes of carbon, $tC\,km^{-2}\,yr^{-1}$ for the Mackenzie River at Tsiigehtchic ($3.8\,^{+1.5}/_{-0.9} \times 10^4$ moles $km^{-2}\,yr^{-1}$), and $0.94\,^{+0.41}/_{-0.26}\,tC\,km^{-2}\,yr^{-1}$, $0.78\,^{+0.35}/_{-0.21}\,tC\,km^{-2}\,yr^{-1}$ and $1.01\,^{+0.42}/_{-0.25}\,tC\,km^{-2}\,yr^{-1}$ for the Peel, Arctic Red and Liard catchments, respectively. When considered alongside published silicate and carbonate weathering rates and the sedimentary burial of biospheric organic carbon, these data suggest that the upper part of the Mackenzie River Basin presently acts as an atmospheric $CO_2$ sink of $\sim 1\,tC\,km^{-2}\,yr^{-1}$ ($\sim 8 \times 10^4$ moles $km^{-2}\,yr^{-1}$) as a result of the carbon transfers by weathering and erosion. During the Last Glacial Maximum, it is possible that the net geochemical carbon balance may have been very different: potential increases in $CO_2$ emissions from oxidative weathering of $OC_{petro}$ and carbonate minerals, coupled with reduced biospheric carbon burial, may have tipped the balance to a net source of $CO_2$.

Keywords: erosion and weathering, carbon cycle, Mackenzie River, petrogenic organic carbon, rhenium

*Department of Earth Sciences, Durham University, Science Laboratories, South Road, Durham, DH1 3LE, United Kingdom
**Department of Geography, Durham University, Science Laboratories, South Road, Durham, DH1 3LE, United Kingdom
***Department of Earth Sciences, Downing Street, University of Cambridge, United Kingdom
§Woods Hole Oceanographic Institute, Woods Hole, Massachusetts, USA
§§Université Paris-Sud, Orsay, France
§§§Institute de Physique du Globe, Paris, France
‡Energy and Environment Institute, University of Hull, Hull, HU6 7RX, United Kingdom
†Corresponding author: khoran@rvc.ac.uk

INTRODUCTION

Erosion and weathering transfer carbon between the atmosphere and lithospheric storage on geological timescales ($10^4$–$10^6$ years). The net carbon balance between carbon dioxide ($CO_2$) sequestration, occurring through silicate weathering by carbonic acid coupled to carbonate precipitation (Ebelmen, 1845; Gaillardet and others, 1999) and the burial of biospheric organic carbon (Berner, 1982; Hayes and Waldbauer, 2006), versus the $CO_2$ release during volcanism (Marty and Tolstikhin, 1998), carbonate weathering by sulphuric acid (Calmels and others, 2007; Torres and others, 2014) and the oxidation of rock-derived organic carbon (Petsch, 2014), governs overall atmospheric $CO_2$ concentrations (Berner and Caldeira, 1997). The organic carbon and sulphur cycles also set atmospheric oxygen concentrations over geological timescales (Berner and Canfield, 1989; Bolton and others, 2006). Although the chemical denudation of silicate minerals and rocks has been studied in detail (for example, Berner and Maasch, 1996; Gaillardet and others, 1999; White and Brantley, 2003; West and others, 2005), the field-based quantification of oxidative weathering of rock-derived organic carbon (petrogenic OC, $OC_{petro}$) remains limited to mountain river catchments in Taiwan (Hilton and others, 2014) and New Zealand (Horan and others, 2017), the floodplains of the Beni River in the Amazon Basin (Bouchez and others, 2010, 2014) and the Ganges and Yamuna Rivers (Dalai and others, 2002; Galy and others, 2008a). Nonetheless, the global $CO_2$ emissions from $OC_{petro}$ oxidation are estimated to be 40–100 Mt C $yr^{-1}$ (Petsch, 2014), which is similar to the $CO_2$ drawdown by chemical weathering of silicate minerals by carbonic acid (Gaillardet and others, 1999; Moon and others, 2014). Improved quantification of these $CO_2$ sources is necessary to constrain the geochemical carbon budgets during weathering and erosion, and to evaluate how long-term changes in tectonics and climate influence atmospheric $CO_2$ (Pagani and others, 2009).

Mountain catchments are thought to be important sites for oxidative weathering (Calmels and others, 2007; Hilton and others, 2014) because high rates of physical erosion, typically in the order of $10^3$–$10^4$ t $km^{-2}$ $yr^{-1}$, can rapidly supply $OC_{petro}$ and sulfides (for example pyrite) to oxygenated surface waters and the atmosphere. The oxidative weathering reactions appear to be able to keep pace with rapid mineral supply, even at high erosion rates (Hilton and others, 2014; Hemingway and others, 2018). As a result, when sedimentary rocks are uplifted in mountain belts, the $CO_2$ released during weathering and erosion can be large (Hilton and others, 2014; Torres and others, 2014; Soulet and others, 2018), and may negate the $CO_2$ sinks by silicate weathering and the burial of recently fixed organic carbon (Torres and others, 2016; Horan and others, 2017). Other features of mountainous topography may result in enhanced rates of $OC_{petro}$ oxidation, including orographic precipitation, high rates of soil formation (Larsen and others, 2014), bedrock landsliding (Emberson and others, 2016), the organic carbon content of the rocks being weathered (Petsch and others, 2000), and a combination of glacial and periglacial processes at higher elevations (Horan and others, 2017).

Here, we quantify carbon fluxes during weathering and erosion in the Mackenzie River Basin, North West Canada, which is a major supplier of water, solutes, sediment and carbon from land to the Arctic Ocean (Carson and others, 1998; Macdonald and others, 1998; Holmes and others, 2002; Millot and others, 2003; Hilton and others, 2015; McClelland and others, 2016). The basin is dominated by Palaeozoic sedimentary rocks, which outcrop in mountain ranges throughout the basin (figs. 1A and 1B) (Millot and others, 2003). Previous work has quantified $CO_2$ drawdown by the erosion and marine burial of biospheric OC (Hilton and others, 2015), silicate weathering (Gaillardet and others, 1999; Millot and others, 2003) and the transient flux of $CO_2$ released when carbonate minerals are weathered by sulfuric acid over timescales that
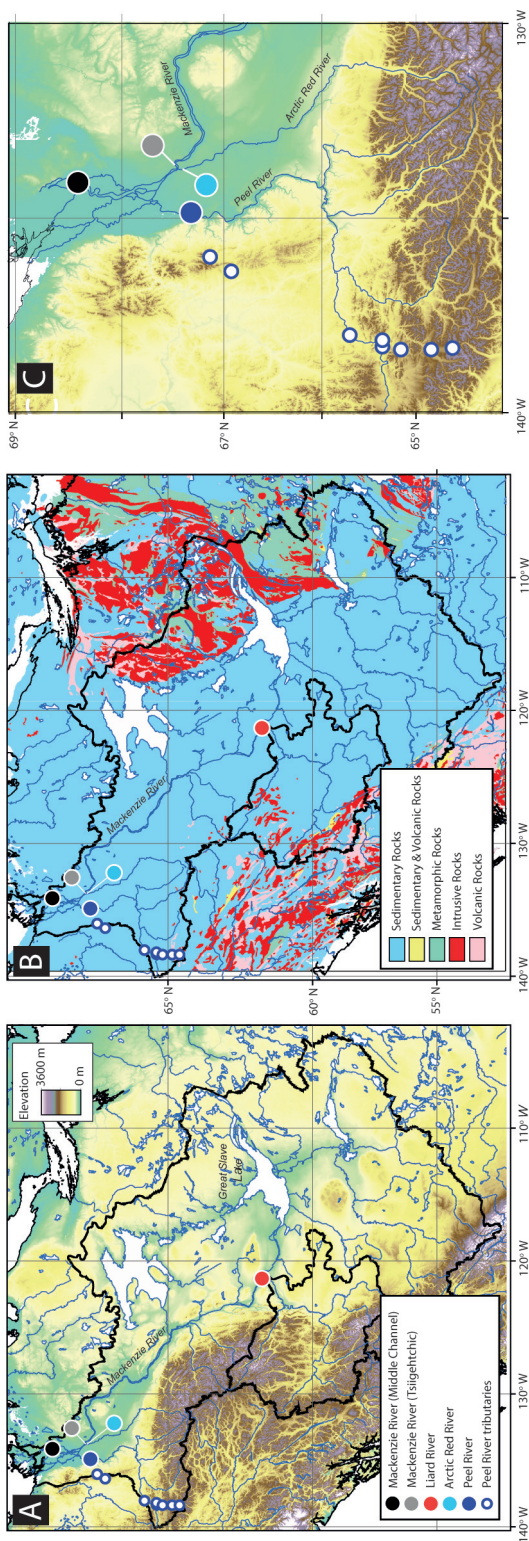
Fig. 1. The Mackenzie River Basin and sampling locations of this study. (A) Elevation (GDEM 30 Arc Second) shown with river sampling locations. Black line is the Mackenzie Basin catchment area and Liard catchment. (B) Bedrock geology of the sampling area, coded by major rock type (Wheeler and others, 1996) . (C) Map of the Mackenzie River delta head and Peel catchment, with sample locations as per part A.

are shorter than that of pyrite burial (over ~10 Ma) (Calmels and others, 2007; Torres and others, 2014). Therefore, this location provides the first opportunity to fully assess the geochemical $CO_2$ budget in a large river basin, which is otherwise understood in terms of its organic and inorganic components, during weathering and erosion. The $CO_2$ budgets we calculate are essential in order to understand how weathering drives the evolution of atmospheric $CO_2$ concentrations and global climate over geological timescales.

### MATERIALS AND METHODS

#### *Approach*

To track chemical weathering, we can assess the products of chemical reactions in the dissolved load of rivers (for example, Meybeck, 1987; Gaillardet and others, 1999; West and others, 2005). River networks can integrate hydrological sources and chemical reaction products, providing a landscape-scale perspective of weathering processes and fluxes (Meybeck, 1987; Gaillardet and others, 1999). Here, we measure dissolved rhenium (Re) concentrations at multiple sites along the Mackenzie River and its tributaries to evaluate $OC_{petro}$ weathering at the catchment scale. Rhenium is considered to be a suitable proxy for determining $OC_{petro}$ oxidation (Dalai and others, 2002) because it is found in close association with $OC_{petro}$ in sedimentary rocks (Selby and Creaser, 2003). When rocks are exposed to chemical weathering, soils developed on sedimentary rocks indicate that Re loss tracks $OC_{petro}$ loss (Jaffe and others, 2002; Hilton and others, 2014; Horan and others, 2017). It is possible to track oxidative weathering by measuring Re in the dissolved load of rivers (Dalai and others, 2002), because this element becomes soluble upon oxidation (Colodner and others, 1993a). If both the dissolved Re flux and the content of Re and $OC_{petro}$ in the rocks undergoing weathering are known, it is possible to quantify the absolute rate of $OC_{petro}$ oxidation (Hilton and others, 2014). Uncertainties in the use of the Re proxy arise from the possibility that phases other than $OC_{petro}$ (for example sulfides and silicate minerals) may supply Re to the dissolved load during weathering (Colodner and others, 1993; Dalai and others, 2002). Therefore, here we assess the relative input of Re from different sources using elemental ratios from dissolved weathering products and solid phases to constrain the $CO_2$ release during $OC_{petro}$ oxidation.

#### *Setting*

The Mackenzie River Basin (fig. 1) spans an area of $1.78 \times 10^6$ km$^2$ upstream of the river delta. It is the largest point source of sediment to the Arctic Ocean (Holmes and others, 2002), including particulate organic carbon (Hilton and others, 2015), and it is the second largest input of dissolved solids (Millot and others, 2003; Calmels and others, 2007). It drains the Rocky and Mackenzie Mountains in north western Canada. From west to east, the Rockies, the interior platform (plains), and the Canadian Shield, which are composed of Precambrian granitic basement, define the basin (Reeder and others, 1972). The basin geology comprises 68.3 percent sedimentary rocks (fig. 1B), including the carbonate platform in the central part, the carbonaceous shales of the interior plain and the Rockies, which are mainly composed of carbonate, dolomitic limestone and shale (Wheeler and others, 1996). The sedimentary rocks host organic carbon (Johnston and others, 2012) and $OC_{petro}$ concentrations inferred from the radiocarbon content of river bed material samples are typically between 0.1 to 0.3 weight percent, but are higher (0.6 wt. %) in the Peel catchment (Hilton and others, 2015). Approximately one third (29.2%) of the basin drains non-sedimentary rocks, including granitic rock outcropping in the Rockies and 2.5 percent of evaporates in the plains (Millot and others, 2003; Beaulieu and others, 2011).
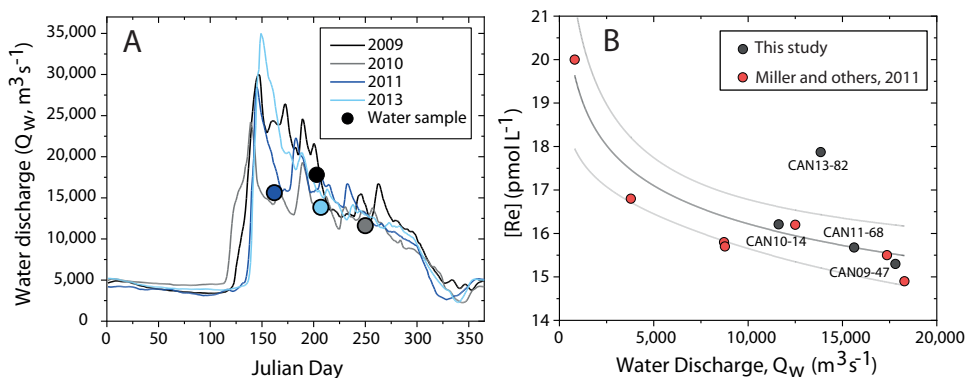
Fig. 2. Hydrometric context for Mackenzie River samples. (A) Hydrographs for the Mackenzie River at Tsiigehtchic over the sampling years 2009, 2010, 2011 and 2013. Daily water discharge ($Q_w$, m$^3$ s$^{-1}$) is shown from Environment Canada (lines) and measurements made at the time of sampling using an Acoustic Doppler Current Profiler are indicated by circles colored based on sample year. (B) Dissolved Re concentration ($[Re]_{diss}$) versus water discharge in the Mackenzie River at Tsiigehtchic. Red circles are data from Miller and others (2011) on samples from the Mackenzie River sampled in March, June, July and August 2004. Samples from this study are shown in gray with the sampling year (for example CAN09) and sample number. The dark gray line shows a power law fit through the data ($[Re]_{diss}$ = $(32.7 \pm 4.5) \times Q_w^{-0.076 \pm 0.015}$, n = 11, r$^2$ = 0.67, $P < 0.001$) and the 95% confidence bands are indicated in light gray.

Weathering of sedimentary rocks dominates the dissolved ion loads in the Mackenzie River (Millot and others, 2003; Calmels and others, 2007; Tank and others, 2016) with an estimated 62 percent of the dissolved inorganic carbon flux derived from carbonate minerals, and 38 percent derived from the atmosphere (Calmels and others, 2007). For the Mackenzie River at Tsiigehtchic (1,680,000 km$^2$), the net $CO_2$ drawdown by silicate weathering (accounting for subsequent carbonate precipitation) is estimated to be 0.26 tC km$^{-2}$ yr$^{-1}$, or $2.2 \times 10^4$ moles km$^{-2}$ yr$^{-1}$ (Gaillardet and others, 1999). Of the carbonate weathering flux, 15 percent is derived from carbonic acid driven weathering and 85 percent from sulphuric acid (via sulfide oxidation) driven weathering (Calmels and others, 2007). The latter reaction drives a net $CO_2$ release of 0.71 tC km$^{-2}$ yr$^{-1}$ ($5.9 \times 10^4$ moles km$^{-2}$ yr$^{-1}$) from carbonate minerals to the atmosphere (Calmels and others, 2007).

In terms of geochemical fluxes associated with the organic carbon cycle, the modern day erosion and export of biospheric organic carbon from soils and vegetation ($OC_{biosphere}$) has been estimated for the upper part of the basin draining north of the Great Slave Lake (fig. 1A), which acts as a sediment trap for particulates eroded from upstream (Carson and others, 1998). Over this 774,200 km$^2$ area, the erosion of $OC_{biosphere}$ is estimated to be 2.9 $^{+1.7}/_{-1.1}$ t C km$^{-2}$ yr$^{-1}$ at the Delta head (Hilton and others, 2015) with a burial efficiency of >65 percent in the Beaufort Sea (Hilton and others, 2015; Vonk and others, 2015); this equates to a $CO_2$ drawdown of ~1.9 tC km$^{-2}$ yr$^{-1}$ (~$16 \times 10^4$ moles km$^2$ yr$^{-1}$). An additional flux of $OC_{petro}$ in the solid load, which has not been oxidized, is estimated to be 0.6 $^{+0.2}/_{-0.2}$ t C km$^{-2}$ yr$^{-1}$ (Hilton and others, 2015).

*Samples*

River samples were collected in July 2009, September 2010, May/June 2011 and July 2013 (fig. 1). They capture periods of high stage and falling water discharge (fig. 2A) when the majority of water and sediment is exported by the Mackenzie River (Carson and others, 1998). Three locations on the main channel of the Mackenzie

*Water discharge measurements by ACDP for sampling periods on the Mackenzie River at Tsiigehtchic*

| Sample ID | Sample date | Water Discharge ($m^3\ s^{-1}$) |
|---|---|---|
| CAN09-47 | 22/07/2009 | 17806 |
| CAN10-14 | 07/09/2010 | 11618 |
| CAN11-68 | 11/06/2011 | 15621 |
| CAN13-82 | 26/07/2013 | 13849 |

River were sampled: the Environment Canada gauging stations at Tsiigehtchic (2009–2011, 2013), the Middle Delta (2010, 2011, 2013) and the main stem at Norman Wells (2010). The main tributaries downstream of the Great Slave Lake, which is an effective sediment trap for materials entering from the lower latitude Rockies (Carson and others, 1998), were sampled: these include the Liard (2009–2011), the Peel (2009–2011, 2013) and the Arctic Red (2009–2011, 2013) rivers. In addition, tributaries of the Peel River (including the Ogilvie and Blackstone rivers) were sampled in 2013 (fig. 1C).

Sample materials include the dissolved products of chemical weathering and the solid products of weathering and erosion carried in suspended load and by river bed materials. River sediment depth-profiles were collected at the main sampling locations to assess the range of erosion products carried by rivers (for example Dellinger and others, 2014; Hilton and others, 2015). Taking multiple samples via river depth profiles addressed the issue that particles become hydro-dynamically sorted in the water column, resulting in a dominant recovery of quartz-rich sediment at the base of the profile and more clay-rich sediments closer to the surface (for example Dellinger and others, 2014; Hilton and others, 2015). In addition, channel depth, water velocity and instantaneous water discharge were measured by two or more transects at each sampling site (fig. 2), using an Acoustic Doppler Current Profiler (ADCP Rio Grande 600 kHz) (table 1). Each water sample (7–8 litres) was transferred into a clean bucket and stored in sterilized and sealable polythene bags. In the upper Peel River tributaries, only surface suspended sediments were collected. Each bag was first weighed to determine the sampled volume, before the water was filtered through 0.2 μm polyether-sulfone (PES) filters within 24 h using pre-cleaned filter units and stored in acid-cleaned LDPE bottles (Hilton and others, 2015). All water samples intended for cation and Re analysis were acidified in the field to pH ~2 following published methods (Dalai and others, 2002; Hilton and others, 2014) and an un-acidified aliquot was kept for anion analyses. River alkalinity was determined shortly after filtration by Gran Titration on an aliquot of filtered water. Suspended sediment was immediately rinsed from the filters using filtered river water and transferred into clean amber-glass vials.

To help constrain the composition of the least weathered portion of the river load, river bed materials were collected at the base of the depth transects from a boat, using a metal bucket as a dredge, and decanted to a sterile bag (Dellinger, ms, 2013; Dellinger and others, 2014; Hilton and others, 2015). In addition, river bank deposits (June 2009 and 2013) were collected from fresh material close to the channel. All sediments were freeze-dried upon return to laboratories within two weeks, weighed and powdered in an agate mill.

*Rhenium Concentration*

Dissolved Re concentrations in the Mackenzie River water samples (table 2), $[Re]_{diss}$, were measured by isotope dilution. A tracer solution enriched in $^{185}Re$ was added to 30 to 100 mL of the water at a volume that would achieve a spike:sample mix ratio between 1.5 and 2.5. The spiked sample was evaporated to dryness. Anion-exchange column chemistry was then used to pre-concentrate the Re and to remove sample matrix: sample was loaded on to 0.5 ml of AG1-X8 (200–400 mesh) Eichrom resin in 0.2 M $HNO_3$, rinsed with 3 ml of 0.2M $HNO_3$, washed with 2 ml of 0.2M HCl and eluted to cleaned PMP beakers in 2.5 mL of 6M $HNO_3$. The purified eluted residues were analyzed by quadrupole inductively-coupled-plasma mass spectrometry (Thermo Scientific X-Series Q-ICP-MS) in 0.8M $HNO_3$. The measured difference in $^{185}Re/^{187}Re$ values for the Re standard solution and the accepted $^{185}Re/^{187}Re$ value (0.5974: Gramlich and others, 1973) was used for mass fractionation correction of the Re sample data. All data were blank corrected. The full procedural blank was $1.35 \pm 0.56$ pg ($\pm 1$ SD, n = 5), which is less than 0.5 percent of the typical sample mass of Re. Uncertainties in the determined Re abundance were calculated by full error propagation of uncertainties in Re mass spectrometer measurements, blank abundance and isotope compositions, spike calibrations and reproducibility of standard Re isotope values. Analysis of $[Re]_{diss}$ in a river water standard, SLRS-5, produced a value of $59.8 \pm 1.7$ ppt (n = 12, $\pm 2$ SE), in agreement with the previously reported value of $66 \pm 12$ ppt (Yeghicheyan and others, 2013).

River water draining solely basaltic igneous rocks was collected from Iceland in 2016 using similar methods (table 3). $[Re]_{diss}$ was determined by direct calibration against a set of seven standards, with varying Re abundances and similar matrixes to the river waters, using Q-ICP-MS (Agilent Technologies 7900). Standards and samples were doped with a known concentration of internal standard Tb and Bi to correct for instrumental drift. The standards confirmed that accuracy and precision was better than 5 percent.

For Re concentration measurements in Mackenzie River sediments (table 4), solid samples were first crushed into fine powders using a zirconium disc mill to achieve an integrated bulk sample. Next, approximately 0.05 g of sediment sample was doped with a known amount of $^{185}Re$ tracer solution and digested in a 6:3 concentrated $HF-HNO_3$ mix (9 mL) for 24 hours at 120 °C and then evaporated. The dried sample was further digested in a 2:1 mix of concentrated $HNO_3-HCl$ (3 mL) for 24 h at 120 °C, and then evaporated to dryness. The Re was isolated and purified using a NaOH-acetone solvent extraction methodology (Cumming and others, 2013). The Re isotope composition of the purified Re aliquots were then determined in a 0.8M $HNO_3$ medium using a Thermo Scientific X-Series Q-ICP-MS and corrected for mass fractionation and blank contributions.

Blanks from the acid digestion protocol ranged from 1–80 pg g$^{-1}$ (n = 19), with typical values between 2 and 8 pg g$^{-1}$ (n = 16); this equates to <0.2 percent of a typical sample concentration (~3000 ppt). Where blanks were high, full-analysis replicates produced data in agreement to within 5 percent, confirming that these blanks were representative of the analysis but had minimal effect on data accuracy. Bush Creek (SBC-1) and SCO-1 standards were used to assess precision. The Re concentration in the Bush Creek standard was quantified to be $10,090 \pm 82$ ppt ($\pm 2$ SE, n = 6) and the Re concentration in the SCO-1 standard is $1085 \pm 55$ ppt ($\pm 2$ SE, n = 6). These values are in agreement with published data on SCO-1 (1050 ppt: Meisel and Moser, 2004) and the long-term in-house reproducibility of the Bush Creek standard by Cr-$H_2SO_4$ dissolution and Negative Thermal Ionisation Mass Spectrometry (N-TIMS) analysis ($10,331.9 \pm 236.9$ ppt, n = 25, $\pm 1$ SD) (this study and Selby unpublished data).

TABLE 2

Major ion and rhenium concentration data for water samples from the Mackenzie River Basin

| Sample name | Collection Date | River | Location | Latitude (deg. N) | Longitude (deg. W) | Water-depth (m) | pH | Temp (°C) | Na* (µmol/L) | K (µmol/L) | Mg (µmol/L) | Ca (µmol/L) | F (µmol/L) | Cl (µmol/L) | $SO_4$ (µmol/L) | Sr (µmol/L) | Li (µmol/L) | $HCO_3^-$ (µmol/L) | Re (pmol/L) |
|---|---|---|---|---|---|---|---|---|---|---|---|---|---|---|---|---|---|---|---|
| CAN09-04 | 15/07/2009 | Liard | Fort Simpson | 61.8357 | 121.2851 | | | | 74.18 | 14.35 | 378.63 | 881.28 | 4.31 | 8.83 | 337.68 | | 0.49 | 1687.76 | 19.12 |
| CAN09-46 | 13/09/2010 | Liard | Fort Simpson | 61.8234 | 121.2976 | | | | 100.11 | 17.78 | 408.00 | 945.87 | 4.60 | 22.38 | 469.69 | | 0.82 | | 23.07 |
| CAN10-48 | 13/09/2010 | Liard | Fort Simpson | 61.8230 | 121.2976 | | | | 98.02 | 17.30 | 402.98 | 922.43 | 4.50 | 21.85 | 471.69 | | 0.83 | | 23.38 |
| CAN09-39 | 21/07/2009 | Peel | Fort MacPherson | 67.3323 | 134.8688 | | | | 138.50 | 14.48 | 622.60 | 1122.87 | 4.52 | 44.93 | 667.13 | | 0.70 | 2162.91 | 15.37 |
| CAN13-01 | 19/07/2013 | Peel | Fort Macpherson | 67.33448 | 134.87762 | 0 | 7.92 | 19.5 | 205.72 | 17.33 | 797.60 | 1451.19 | | 42.22 | 966.90 | 3.03 | 0.56 | 2587.82 | 25.75 |
| CAN13-81 | 26/07/2013 | Peel | Fort Macpherson | 67.33448 | 134.87762 | 3.5 | | | 159.04 | 12.68 | 690.40 | 1162.18 | | 36.51 | 797.14 | 2.68 | 0.46 | 2350.30 | 19.31 |
| CAN11-79 | 11/06/2011 | Peel | Fort Macpherson | 67.33448 | 134.87762 | | | | 141.76 | 16.90 | 625.71 | 1080.20 | 3.75 | 48.15 | 705.17 | 1.39 | 0.79 | | 15.94 |
| CAN09-07 | 16/07/2009 | Mackenzie | Fort Simpson | 61.85104 | 121.27722 | | | | 149.25 | 22.96 | 258.67 | 673.76 | 3.02 | 197.33 | 226.77 | | 0.46 | 1438.94 | 11.54 |
| CAN09-47 | 22/07/2009 | Mackenzie | Tsiigehtchic | 67.4584 | 133.7233 | | | | 122.13 | 19.08 | 364.92 | 822.16 | 5.89 | 145.66 | 365.40 | | 0.53 | 1564.45 | 15.30 |
| CAN10-14 | 7/09/2010 | Mackenzie | Tsiigehtchic | 67.4580 | 133.7270 | | | | 146.39 | 22.19 | 462.04 | 1020.98 | 5.38 | 196.66 | 461.04 | 2.12 | 0.63 | | 16.21 |
| CAN11-68 | 11/06/2011 | Mackenzie | Tsiigehtchic | | | | | | 110.14 | 23.03 | 312.09 | 778.16 | 3.86 | 131.34 | 304.83 | 1.75 | 0.54 | | 15.68 |
| CAN13-82 | 26/07/2013 | Mackenzie | Tsiigehtchic | 67.45818 | 133.72734 | 5 | | | 133.59 | 19.23 | 398.33 | 868.36 | | 188.97 | 451.03 | 3.28 | 0.32 | 1918.43 | 17.87 |
| CAN13-65 | 24/07/2013 | Mackenzie | Delta Middle Channel, Inuvik | 68.41313 | 134.08893 | 6 | 8.04 | 16.9 | 123.64 | 18.29 | 384.71 | 842.04 | | 163.42 | 454.22 | 3.20 | 0.30 | 1973.48 | 19.57 |
| CAN10-26 | 8/09/2010 | Mackenzie | Delta Middle Channel, Inuvik | 68.4343 | 134.2222 | | | | 158.76 | 21.74 | 460.50 | 991.26 | 4.21 | 167.38 | 444.51 | 2.34 | 0.73 | | 17.90 |
| CAN11-100 | 14/06/2011 | Mackenzie | Delta Middle Channel, Inuvik | | | | | | 197.25 | 21.51 | 291.08 | 713.16 | | | | 1.51 | 0.52 | | 15.01 |
| CAN09-50 | 22/07/2009 | Arctic Red | Tsiigehtchic | 67.4261 | 133.7787 | | | | 143.35 | 21.68 | 570.39 | 1152.73 | 5.72 | 16.15 | 854.42 | | 0.95 | 1552.23 | 22.46 |
| CAN10-18 | 7/09/2010 | Arctic Red | Tsiigehtchic | 67.4396 | 133.7553 | | | | 133.08 | 18.58 | 840.25 | 1382.91 | 4.52 | 23.55 | 1141.46 | 1.62 | 0.88 | | 13.96 |
| CAN13-83 | 26/07/2013 | Arctic Red | Tsiigehtchic | | | 0.3 | | | 120.48 | 15.54 | 759.36 | 1217.25 | | 15.08 | 1057.73 | 2.75 | 0.49 | 2161.63 | 18.16 |
| CAN13-09 | 20/07/2013 | Ogilvie | First Dempster sight | 65.71532 | 137.99249 | 0 | 8.1 | 12.1 | 400.80 | 12.16 | 776.69 | 1561.40 | | 91.79 | 1051.88 | 3.61 | 1.57 | 2674.45 | 34.80 |
| CAN13-12 | 20/07/2013 | Ogilvie | Dempster Bridge | 65.36131 | 138.17824 | 0 | 8.26 | 12.9 | 521.85 | 11.32 | 691.58 | 1249.46 | | 73.13 | 1147.58 | 3.44 | 1.54 | 2702.91 | 27.92 |
| CAN13-33i | 22/07/2013 | Ogilvie | Dempster | 65.36216 | 138.30226 | 0 | 7.81 | 13.8 | 513.38 | 9.68 | 525.63 | 940.27 | | 22.22 | 861.89 | 2.80 | 0.84 | 1818.83 | 21.88 |
| CAN13-33ii | 22/07/2013 | Ogilvie | Dempster Bridge | 65.36216 | 138.30226 | 0 | 7.81 | 13.8 | | | | | | | | | | | |
| CAN13-05 | 19/07/2013 | Eagle | Nr Eagle Plains | 66.44326 | 136.71062 | 0 | 7.44 | 13.9 | 619.13 | 19.37 | 809.37 | 1401.04 | | 19.33 | 1978.73 | 3.07 | 1.14 | 1256.21 | 39.83 |
| CAN13-13 | 20/07/2013 | Engineer Creek | Dempster Bridge | 65.35699 | 123.29301 | 0 | 8.08 | 12.2 | 229.06 | 21.91 | 1210.06 | 2534.39 | | 329.31 | 3070.56 | 7.69 | 4.48 | 2834.50 | 76.50 |
| CAN13-29 | 22/07/2013 | Upper Engineer Creek | Dempster | 65.10129 | 138.35582 | 0 | 6.98 | 9.2 | 85.87 | 15.23 | 893.66 | 3019.72 | | 37.71 | 1881.58 | 6.14 | 1.02 | 3412.29 | 99.89 |
| CAN13-30 | 22/07/2013 | Upper Engineer Creek (upstream Red Creek) | Dempster | 65.17129 | 138.36353 | 0 | 6.99 | 10.3 | 65.61 | 12.89 | 902.38 | 2025.11 | | 33.85 | 2202.97 | 4.58 | 0.97 | 2296.26 | 80.56 |
| CAN13-14 | 20/07/2013 | Blackstone | Dempster Bridge | 64.60593 | 138.34065 | 0 | 7.77 | 10.6 | 155.83 | 12.75 | 1174.57 | 1353.20 | | 5.31 | 2280.78 | 5.02 | 0.56 | 1394.00 | 14.40 |
| CAN13-25 | 22/07/2013 | West Blackstone | Dempster Bridge | 64.83523 | 138.36215 | 0 | 7.75 | 11 | 77.50 | 12.24 | 529.57 | 886.71 | | 12.17 | 710.71 | 2.55 | 0.17 | 1628.13 | 14.69 |
| CAN13-45 | 23/07/2013 | Rock | Dempster | 66.91653 | 136.34325 | 0 | 7.89 | 9 | 25.50 | 8.60 | 690.98 | 1884.46 | | 9.55 | 1124.15 | 3.42 | 0.13 | 2890.43 | 14.49 |
| CAN13-47 | 23/07/2013 | James Creek | Dempster | 67.13862 | 136.00302 | 0 | 6.97 | 9.3 | 546.51 | 21.17 | 1132.31 | 866.52 | | 4.85 | 2288.50 | 2.96 | 0.45 | 95.77 | 1.46 |

Na* indicates the Na concentration that has been corrected for atmospheric inputs.

TABLE 3

*River water samples from Iceland*

| Sample_ID* | Latitude | Longitude | $[Re]_{diss}$ pmol/L | $[Re]/[Na*]$ (pmol/μmol) | $[Re]/[SO_4]$ (pmol/μmol) |
|---|---|---|---|---|---|
| A8 | 64.6935 | 21.4145 | 2.22 | 0.0320 | 0.266 |
| A12 | 64.7062 | 21.0392 | 1.32 | 0.00618 | 0.118 |
| A14 | 64.6552 | 20.7011 | 0.46 | 0.00453 | 0.0487 |
| G1 | 64.7039 | 20.9929 | 1.86 | 0.00812 | 0.172 |
| G2 | 64.7039 | 20.9929 | 1.68 | 0.00557 | 0.122 |
| G3 | 64.7152 | 20.8339 | 1.05 | 0.00688 | 0.144 |

*From von Strandmann and others, 2008.

### Major Ion and Elemental Concentrations

Major ion concentrations in water samples were analyzed by Ion Chromatography. Cation and anion standards and a certified reference standard (Lethbridge-03) were run to validate the analytical results. Major and trace element (other than Re) concentrations in the river sediment samples were measured, respectively, by ICP-AES and ICP-MS at the SARM (Service d'Analyse des Roches et des Minéraux, INSU facility, Vandoeuvre-les-Nancy, France). In river bed materials and suspended load sediments from 2013, the organic carbon concentration ([OC], %) was measured following a 0.2M HCl leach protocol (Galy and others, 2007), which was tested on samples from this location to ensure full removal of detrital carbonates. Aliquots of samples were combusted and the concentration and stable isotope composition of OC ($\delta^{13}C$, ‰) was determined using a Costech elemental analyzer coupled to a Thermo Scientific Delta V Advantage isotope ratio mass spectrometer (EA-IRMS). Corrections for procedural and instrumental blanks were applied and the result normalized to the composition of international standards (reported relative to VPDB, with a precision of 0.2‰).

### Previously Published Data

Major ion analyses on the dissolved load of the 2013 samples from this study supplement published major ion data for the 2009 and 2011 samples that have been described previously (Dellinger, ms, 2013). This study also takes advantage of published data on particulate organic carbon (POC), including the organic carbon (OC) percentage, $\delta^{13}C$, and the radiocarbon activity, reported as Fraction Modern, $F^{14}C$, as per Reimer and others (2004), from suspended sediment and bed material samples collected in 2009 and 2011 (Hilton and others, 2015) (note $F^{14}C$ is the same notation as $F_{mod}$ reported in Hilton and others, 2015). These data were acquired using a HCl fumigation method, so elemental and isotope compositions may not be directly comparable to the additional %OC and $\delta^{13}C$ from this study (table 4). We also make use of sedimentary rock samples collected from drill cores in the Western Canadian Sedimentary Basin (Ross and Bustin, 2009), close to the Liard River sampling point (fig. 1). These are mostly Devonian to Mississippian shales, which are common throughout the wider basin. The Lower and Upper Besa Shale unit samples provide the broadest range across the regional stratigraphy (Ross and Bustin, 2009). We exclude samples from that dataset where [Re] values were below the detection limit of that study: <2 ppb (table 5).

### RESULTS

### Bulk Weathering Characteristics

The concentrations of $HCO_3^-$, $Ca^{2+}$ and $Mg^{2+}$ normalized to $Na^+$ are helpful for characterizing overall weathering processes (Gaillardet and others, 1999). Following

TABLE 4

*Geochemical composition of river sediments*

| Sample ID | River | Location | Date | Latitude | Longitude | Sample type | Sample Water Depth (m) | Suspended Sediment Concentration (mg/L) | [OC] (%) | Ref.* | $\delta^{13}C_{org}$ (permil) | Ref.* | $F^{14}C$ | Al (ppm) | Na (ppm) | Si (ppm) | Re (ppt) |
|---|---|---|---|---|---|---|---|---|---|---|---|---|---|---|---|---|---|
| CAN09-11 | Liard | Fort Simpson | 16/07/2009 | 61.8423 | 121.2957 | **BL | Thalweg | - | 0.14 | / | -28.2 | / | 0.155 | 28744 | 5816 | 350604 | 1405 |
| CAN10-50 | Liard | Fort Simpson | 13/09/2010 | 61.8234 | 121.2976 | BL | 3.5 | 542 | 1.51 | / | -26.4 | / | 0.465 | 26796 | 6803 | 384839 | 862 |
| CAN11-05 | Liard | Fort Simpson | 4/06/2011 | 61.8234 | 121.2976 | ***spm | 4.8 | 492 | 1.49 | / | -26.6 | / | 0.633 | 55058 | 5059 | 274805 | 2515 |
| CAN10-46 | Liard | Fort Simpson | 13/09/2010 | 61.8234 | 121.2976 | spm | 6.5 | 490 | 1.43 | / | -26.4 | / | 0.481 | 38265 | 5712 | 336460 | 2283 |
| CAN11-03 | Liard | Fort Simpson | 4/06/2011 | 61.8234 | 121.2976 | spm | 0 | 438 | 1.47 | / | -26.4 | / | 0.452 | 56524 | 5200 | 275974 | 2667 |
| CAN11-07 | Liard | Fort Simpson | 4/06/2011 | 61.8234 | 121.2976 | spm | 0 | | | / | | / | | 58509 | 5015 | 264288 | 2986 |
| CAN09-41 | Peel | Fort MacPherson | 21/07/2009 | 67.3319 | 134.8691 | BL | | | | / | | / | | 40620 | 2708 | 342723 | 4356 |
| CAN13-02 | Peel | Fort Macpherson | 19/07/2013 | 67.33448 | 134.8776 | Bank | | | 1.44 | this study | -26.6 | this study | | | | | 4122 |
| CAN13-03 | Peel | Fort Macpherson | 19/07/2013 | 67.33448 | 134.8776 | Bank-wood | | | 19.40 | this study | -27.0 | this study | | | | | 6936 |
| CAN10-03 | Peel | Fort MacPherson | 7/09/2010 | 67.3313 | 134.8656 | spm | 8.5 | 250 | 2.00 | / | -26.8 | / | 0.383 | 58694 | 3338 | 305188 | 3538 |
| CAN10-06 | Peel | Fort MacPherson | 7/09/2010 | 67.3313 | 134.8656 | spm | 0 | 101 | 2.24 | / | -26.8 | / | 0.284 | 76053 | 3487 | 277376 | 3587 |
| CAN10-07 | Peel | Fort MacPherson | 7/09/2010 | 67.3313 | 134.8656 | BL | Thalweg | - | 0.75 | / | -28.0 | / | 0.133 | 34205 | 2982 | 360439 | 2478 |
| CAN11-77 | Peel | Fort MacPherson | 11/06/2011 | 67.3313 | 134.8656 | spm | 6 | 325 | 2.27 | / | -26.8 | / | 0.480 | 58519 | 3680 | 285790 | 4817 |
| CAN11-79 | Peel | Fort MacPherson | 11/06/2011 | 67.3313 | 134.8656 | spm | 0 | 146 | 1.85 | / | -26.6 | / | 0.315 | 72153 | 4028 | 267139 | 4729 |
| CAN09-48 | Mackenzie | Tsiigehtchic | 22/07/2009 | 67.4494 | 133.7406 | BL | Thalweg | - | 0.16 | / | -28.0 | / | | 27225 | 5490 | 342499 | 740 |
| CAN10-16 | Mackenzie | Tsiigehtchic | 7/09/2010 | 67.4530 | 133.7405 | BL | Thalweg | - | 1.42 | / | -26.6 | / | 0.162 | 27913 | 6766 | 358803 | 747 |
| CAN10-15 | Mackenzie | Tsiigehtchic | 7/09/2010 | 67.4530 | 133.7405 | spm | 0 | 231 | 1.42 | / | -26.4 | / | 0.354 | 83833 | 3487 | 242552 | 2876 |
| CAN11-65 | Mackenzie | Tsiigehtchic | 11/06/2011 | 67.4530 | 133.7405 | spm | 13 | 941 | 1.62 | / | -26.4 | / | 0.570 | 39509 | 5512 | 312667 | 1894 |
| CAN11-66 | Mackenzie | Tsiigehtchic | 11/06/2011 | 67.4530 | 133.7405 | spm | 10 | 445 | 1.40 | / | -26.6 | / | 0.444 | 50607 | 5089 | 291446 | 2069 |
| CAN11-67 | Mackenzie | Tsiigehtchic | 11/06/2011 | 67.4530 | 133.7405 | spm | 5 | 322 | 1.43 | / | -26.6 | / | 0.456 | 56614 | 4436 | 264428 | 2357 |
| CAN11-68 | Mackenzie | Tsiigehtchic | 11/06/2011 | 67.4530 | 133.7405 | spm | 0 | 291 | 1.54 | / | -26.5 | / | 0.451 | 59948 | 4281 | 260268 | 2642 |
| CAN13-62 | Mackenzie | Delta Middle Channel | 24/07/2013 | 68.41313 | 134.0889 | Bank-0.5m | | | 0.84 | this study | -27.0 | this study | | | | | 1966 |
| CAN13-63 | Mackenzie | Delta Middle Channel | 24/07/2013 | 68.41313 | 134.0889 | Bank-1.0m | | | 2.32 | this study | -27.2 | this study | | | | | 2652 |
| CAN13-64 | Mackenzie | Delta Middle Channel | 24/07/2013 | 68.41313 | 134.0889 | Bank-1.5m | | | 1.29 | this study | -26.6 | this study | | | | | 2723 |
| CAN10-28 | Mackenzie | Delta Middle Channel | 9/09/2010 | 68.4092 | 134.0805 | spm | 19 | 513 | 1.42 | / | -26.7 | / | 0.419 | 56947 | 4229 | 276161 | 2105 |
| CAN10-27 | Mackenzie | Delta Middle Channel | 8/09/2010 | 68.4457 | 134.2135 | BL | | | | / | | / | | 32290 | 4740 | 309115 | 1498 |
| CAN11-89 | Mackenzie | Delta Middle Channel | 13/06/2010 | 68.4092 | 134.0805 | spm | 8 | 240 | 1.54 | / | -26.5 | / | 0.401 | 62302 | 4507 | 261837 | 2794 |
| CAN10-29 | Mackenzie | Delta Middle Channel | 9/09/2010 | 68.4092 | 134.0805 | spm | 17 | 275 | 1.49 | / | -26.6 | / | 0.377 | 77165 | 3635 | 250498 | 2949 |
| CAN10-32 | Mackenzie | Delta Middle Channel | 9/09/2010 | 68.4092 | 134.0805 | BL | 0 | 162 | 1.42 | / | -26.6 | / | 0.307 | 90608 | 3264 | 238298 | 3003 |
| CAN10-38 | Mackenzie | Delta Middle Channel | 9/09/2010 | 68.4092 | 134.0805 | BL | Thalweg | - | 0.37 | / | -28.0 | / | 0.120 | 32258 | 5037 | 326363 | 1261 |
| CAN11-87 | Mackenzie | Delta Middle Channel | 13/06/2011 | 68.4092 | 134.0805 | spm | 20 | 848 | 2.71 | / | -26.5 | / | 0.568 | 43895 | 4440 | 278898 | 3595 |
| CAN11-88 | Mackenzie | Delta Middle Channel | 13/06/2011 | 68.4092 | 134.0805 | spm | 15 | 850 | 1.00 | / | -26.6 | / | 0.366 | 42215 | 4662 | 293562 | 1805 |
| CAN09-53 | Arctic Red | Tsiigehtchic | 22/07/2009 | 67.4261 | 133.7787 | BL | | | | / | | / | | 45330 | 2960 | 300177 | 3380 |
| CAN10-20 | Arctic Red | Tsiigehtchic | 7/09/2010 | 67.4395 | 133.7530 | BL | | | | / | | / | | 47146 | 3539 | 290371 | 4099 |
| CAN10-17 | Arctic Red | Tsiigehtchic | 7/09/2010 | 67.4394 | 133.7529 | spm | 6 | 123 | 2.17 | / | -26.8 | / | 0.299 | 73830 | 3042 | 251246 | 7214 |
| CAN10-19 | Arctic Red | Tsiigehtchic | 7/09/2010 | 67.4394 | 133.7529 | spm | 0 | 123 | 1.95 | / | -26.8 | / | 0.291 | 71608 | 3042 | 251246 | 7145 |
| CAN13-10 | Ogilvie | Along Dempster | 20/07/2013 | 65.56789 | 138.1782 | Bank | | | 0.90 | this study | -28.3 | this study | | | | | 11354 |
| CAN13-11 | Ogilvie | Along Dempster | 20/07/2013 | 65.45345 | 138.2198 | Bedrock-Lignite | | | 3.29 | this study | -31.4 | this study | | | | | 321459 |

TABLE 4

*(continued)*

| Sample ID | River | Location | Date | Latitude | Longitude | Sample type | Sample Water Depth (m) | Suspended Sediment Concentration (mg/L) | [OC] (%) | Ref.* | $\delta^{13}$Corg (permil) | Ref.* | $F^{14}$C | Al (ppm) | Na (ppm) | Si (ppm) | Re (ppt) |
|---|---|---|---|---|---|---|---|---|---|---|---|---|---|---|---|---|---|
| CAN13-07 | Eagle River | Nr Eagle Plains | 19/07/2013 | 66.44326 | 136.7106 | Bank | | | 1.48 | | -26.5 | this study | | | | | 4453 |
| CAN13-28 | Upper Engineer Creek | Dempster | 22/07/2013 | 65.10129 | 138.3558 | Bank | | | 3.18 | | - | this study | | | | | 13315 |
| CAN13-31 | Upper Engineer Creek (upstream Red Creek) | Dempster | 22/07/2013 | 65.17129 | 138.3635 | Bank | | | 1.35 | | -28.9 | this study | | | | | 13343 |
| CAN13-32 | Upper Engineer Creek (upstream Red Creek) | Dempster | 22/07/2013 | 65.17129 | 138.3635 | Bank (orange mat) | | | 1.67 | | -18.3 | this study | | | | | 12618 |
| CAN13-14 | Blackstone | Dempster bridge | 20/07/2013 | 64.60593 | 138.3407 | Bank | | | 2.92 | | -27.8 | this study | | | | | 25064 |
| CAN13-15 | Blackstone | Dempster bridge | 20/07/2013 | 64.60593 | 138.3407 | Bank | | | 0.93 | | -26.8 | this study | | | | | 2488 |
| CAN13-24 | West Blackstone | Dempster bridge | 22/07/2013 | 64.83523 | 138.3622 | Bedload-dredge | | | 0.29 | | -27.1 | this study | | | | | 1050 |
| CAN13-44 | Rock | Dempster | 23/07/2013 | 66.91653 | 136.3433 | Bank | | | 1.12 | | -29.6 | this study | | | | | 8669 |
| CAN13-48 | Unnamed | Dempster | 23/07/2013 | 67.13862 | 136.003 | Bank | | | 0.68 | | -27.5 | this study | | | | | 2737 |

*Reference *1* = Hilton and others, 2015.
**BL = bedload; ***spm = suspended particulate matter.

TABLE 5

*Insight on Re source in solid materials from published studies*

| Sample type | Details/Sample ID | Reference | n | [OC] % | [S] % | [Re] pmol/g | ±SE pmol/g | [Re]/[Na] pmol/µmol | ±SE pmol/µmol | [Re]/[S] pmol/µmol | ±SE pmol/µmol |
|---|---|---|---|---|---|---|---|---|---|---|---|
| Silicate minerals | Peridotite (massive and xenolith) | Pearson and others, 2004 | 47 | n.d. | 0.01 | 0.64 | 0.09 | 0.0236 | 0.0038 | 0.295 | 0.048 |
| Silicate minerals | Spinel-lherzolite | Burton and others, 1999 | 1 | n.d. | 0.01 | 0.63 | | 0.0038 | | 0.183 | |
| Silicate minerals | Basalts | Burton and others, 2002 | 3 | n.d. | n.d. | 3.83 | 0.34 | 0.0039 | 0.0006 | | |
| Silicate minerals | Peridotites | Reisberg and Lorand, 1995 | 11 | n.d. | 0.02 | 0.96 | 0.19 | 0.0256 | 0.0133 | 0.179 | 0.028 |
| OCpetro | Coals and siliciclastic rocks (GC formation) | Dai and others, 2015 | 8 | 84.5 | 6.6 | 3477 | 2 | 230.9 | 81.2 | 1.985 | 0.987 |
| OCpetro | Coals and siliciclastic rocks (HST formation) | Dai and others, 2015 | 7 | 78.8 | 6.1 | 667 | 5 | 45.2 | 10.7 | 0.352 | 0.086 |
| Sedimentary rock | LBR3 25-1 | Ross and Bustin, 2009 | 1 | 2 | 2.3 | 59 | | 0.96 | | 0.082 | |
| Sedimentary rock | LBR3 25-3 | Ross and Bustin, 2009 | 1 | 2 | 1.1 | 59 | | 0.96 | | 0.172 | |
| Sedimentary rock | LBR3 25-5 | Ross and Bustin, 2009 | 1 | 2.1 | 1.7 | 91 | | 1.41 | | 0.172 | |
| Sedimentary rock | LBR25 63-1 | Ross and Bustin, 2009 | 1 | 4.8 | 1.2 | 226 | | 13.98 | | 0.603 | |
| Sedimentary rock | LBR25 63-3 | Ross and Bustin, 2009 | 1 | 4.4 | 1.7 | 209 | | 10.82 | | 0.395 | |
| Sedimentary rock | LBR25 63-5 | Ross and Bustin, 2009 | 1 | 2.8 | 1.7 | 134 | | 6.93 | | 0.253 | |
| Sedimentary rock | LBR25 63-7 | Ross and Bustin, 2009 | 1 | 2.5 | 1.4 | 118 | | 36.61 | | 0.271 | |
| Sedimentary rock | UBR-C15-1331-1 | Ross and Bustin, 2009 | 1 | 1.4 | 1.3 | 59 | | 0.57 | | 0.146 | |
| Sedimentary rock | UBR-C15-1331-5 | Ross and Bustin, 2009 | 1 | 4 | 1.6 | 252 | | 2.11 | | 0.506 | |
| Sedimentary rock | UBR-C15-1331-7 | Ross and Bustin, 2009 | 1 | 2.2 | 2.2 | 129 | | 0.95 | | 0.188 | |
| Sedimentary rock | UBR 1331-1 | Ross and Bustin, 2009 | 1 | 2 | 2.1 | 38 | | 0.15 | | 0.057 | |
| Sedimentary rock | UBR 1331-3 | Ross and Bustin, 2009 | 1 | 2.7 | 2.2 | 75 | | 0.35 | | 0.110 | |
| Sedimentary rock | UBR 1331-4 | Ross and Bustin, 2009 | 1 | 4 | 3.4 | 43 | | 0.13 | | 0.041 | |
| Sedimentary rock | UBR 1331-8 | Ross and Bustin, 2009 | 1 | 5.7 | 4.5 | 48 | | 0.19 | | 0.034 | |
| Sedimentary rock | UBR1331-11 | Ross and Bustin, 2009 | 1 | 3.8 | 4.4 | 38 | | 0.16 | | 0.027 | |
| Sedimentary rock | MU1745-1 | Ross and Bustin, 2009 | 1 | 1.9 | 2.6 | 86 | | 0.70 | | 0.106 | |
| Sedimentary rock | MU1745-2 | Ross and Bustin, 2009 | 1 | 1.9 | 3.6 | 134 | | 1.07 | | 0.120 | |
| Sedimentary rock | MU1745-3 | Ross and Bustin, 2009 | 1 | 2.3 | 4.5 | 172 | | 1.27 | | 0.122 | |
| Sedimentary rock | MU1745-4 | Ross and Bustin, 2009 | 1 | 2 | 4.3 | 263 | | 4.29 | | 0.196 | |
| Sedimentary rock | MU414-1 | Ross and Bustin, 2009 | 1 | 3.7 | 1.4 | 451 | | 2.69 | | 1.033 | |
| Sedimentary rock | MU414-2 | Ross and Bustin, 2009 | 1 | 3.6 | 1.8 | 806 | | 5.55 | | 1.435 | |
| Sedimentary rock | MU414-3 | Ross and Bustin, 2009 | 1 | 2.5 | 4.4 | 360 | | 1.47 | | 0.262 | |
| Sedimentary rock | MU414-4 | Ross and Bustin, 2009 | 1 | 1.4 | 1.7 | 48 | | 0.16 | | 0.091 | |
| Sedimentary rock | MU714-1 | Ross and Bustin, 2009 | 1 | 3.3 | 1.7 | 75 | | 0.90 | | 0.142 | |
| Sedimentary rock | MU714-2 | Ross and Bustin, 2009 | 1 | 2.8 | 1.7 | 204 | | 1.62 | | 0.385 | |
| Sedimentary rock | MU1416-1 | Ross and Bustin, 2009 | 1 | 2.1 | 2.2 | 140 | | 0.77 | | 0.204 | |
| Sedimentary rock | MU1416-3 | Ross and Bustin, 2009 | 1 | 2.1 | 2.2 | 242 | | 1.31 | | 0.352 | |
| Sedimentary rock | MU1416-7 | Ross and Bustin, 2009 | 1 | 2 | 2.4 | 328 | | 2.03 | | 0.438 | |
| Sedimentary rock | FS1238-12 | Ross and Bustin, 2009 | 1 | 0.32 | 2.15 | 414 | | 3.20 | | 0.617 | |

Millot and others (2003), all Na data has been corrected for any cyclic input of ocean-derived Na input by precipitation, based on the conservative behavior of chlorine, and is given as Na*; where $[Na]^* = [Na] - 0.85 \times [Cl]$. The major ion chemistry of the 2009–2011 dissolved load samples is similar to the major ion data from the 2013 dissolved load samples and previous measurements from the Mackenzie River Basin and supports the important role of sedimentary rocks in setting the dissolved load chemistry (Millot and others, 2003). Sulfate concentrations are elevated in the Peel tributaries, with a mean $[SO_4^{2-}] = 1691 \pm 454 \, \mu mol \, L^{-1}$ (n = 11, ±2 SE), relative to the main Mackenzie channel, where mean $[SO_4^{2-}] = 396 \pm 74 \, \mu mol \, L^{-1}$ (n = 4, ±2 SE), in agreement with samples from 1996 (Millot and others, 2003). The oxidative weathering of sulfide minerals generates sulfuric acid that can subsequently weather carbonate minerals; this has been shown previously in the basin (Calmels and others, 2007). The high reaction kinetics of sulfide oxidation and carbonate weathering, compared with silicate weathering, can help to explain the relative enrichment in Ca, Mg and $HCO_3^-$ in the Peel River catchment.

*Dissolved Rhenium Concentration and Flux*

The concentrations of dissolved Re, $[Re]_{diss}$, in the Mackenzie River Basin range from 1.46–85.7 pmol $L^{-1}$ across the sample set (table 2), but there is much less variability at a given sample location. In the main stem of the Mackenzie River at Tsiigehtchic, the mean $[Re]_{diss} = 16.3 \pm 1.1$ pmol $L^{-1}$ (n = 4, ±2 SE, from this point ±2 standard errors unless otherwise stated), which falls within the range reported by Miller and others (2011) at the same location. Dissolved Re concentration values for the Mackenzie River Basin fall towards the more concentrated end of published data from global rivers of $4.7 \pm 0.2$ pmol $L^{-1}$ to $25.4 \pm 1.2$ pmol $L^{-1}$ (Colodner and others, 1993; Dalai and others, 2002; Miller and others, 2011; Rahaman and others, 2012; Hilton and others, 2014). For the Mackenzie River at the delta, the mean $[Re]_{diss}$ is $17.5 \pm 2.7$ pmol $L^{-1}$ (n = 3). The mean $[Re]_{diss}$ concentrations of the Liard ($21.9 \pm 2.7$ pmol $L^{-1}$, n = 3), Peel ($19.0 \pm 4.8$ pmol $L^{-1}$, n = 4) and Arctic Red ($18.2 \pm 4.9$, n = 3) catchments are higher. The greatest variation in $[Re]_{diss}$ is observed in the tributaries feeding the Peel River. Engineer Creek has a mean $[Re]_{diss}$ of $85.7 \pm 14.4$ pmol $L^{-1}$ (n = 3), which is the highest concentration measured across the Mackenzie River Basin.

To calculate dissolved Re fluxes (g $yr^{-1}$) and yields (g $km^{-2} \, yr^{-1}$) at the main sampling sites, $[Re]_{diss}$ was examined alongside measurements of water discharge, $Q_w$ $m^3 \, s^{-1}$ (fig. 2). Published and new measurements for the Mackenzie River at Tsiigehtchic show a decrease in $[Re]_{diss}$ with increasing $Q_w$ (fig. 2B). Note we do not correct $[Re]_{diss}$ for rainwater inputs, due to the very low [Re]/[Cl] ratio of seawater (Colodner and others, 1993) and rainwater samples collected away from anthropogenic pollution sources (Miller and others, 2011; Horan and others, 2017). At Tsiigehtchic, the relationship between $[Re]_{diss}$ and $Q_w$ is well described by a power law function ($r^2 = 0.7$), where $[Re]_{diss} = (32.7 \pm 4.5) \times Q_w^{-0.076 \pm 0.015}$. This relationship can be used to estimate $[Re]_{diss}$ from gauged measurements of daily discharge from the Mackenzie River (Environment Canada data, accessed online, 10/05/17).

Weathering fluxes are calculated as the product of discharge and element concentration, and we use the relationship between Re concentration and discharge to estimate total annual dissolved Re flux over the time period 2009–2013 for the Mackenzie River at Tsiigehtchic. This method estimates that the dissolved Re fluxes are similar between 2009 and 2013; varying from 4637 to 5309 mol $yr^{-1}$. Using the average measured $[Re]_{diss}$ and average annual discharge calculated over the years 2009–2013 gives a dissolved Re flux that is within 10 percent of the power law rating curve method. This suggests that an average method provides an accurate reflection of the dissolved Re flux through time in this catchment. For the other gauging stations (Liard, Peel,

Arctic Red), insufficient samples were available to constrain a relationship between $[Re]_{diss}$ and $Q_w$ and so average $[Re]_{diss}$ values were used to calculate mean annual dissolved Re flux from long-term $Q_w$ measurements.

### River Bed Materials and Suspended Sediments

*Re concentration.*—In the Liard catchment, the Re concentration in river bed materials, $[Re]_{BM}$, is 1405 ppt and 862 ppt (table 4). The $[Re]_{BM}$ in the main channel of the Mackenzie River at Tsiigehtchic is 740 ppt and 747 ppt. Concentrations downstream at the Mackenzie delta are more than double this at 2020 ± 591 ppt (n = 5). The higher concentrations in the delta coincide with the additional contribution of sediments from the Peel and Arctic Red catchments (Carson and others, 1998; Carson and others, 1999). Huh and others (2004) find a $[Re]_{BM}$ = 5019 ppt in the Arctic Red and $[Re]_{BM}$ = 3922 ppt in the Peel. Here, in the Arctic Red catchment we measure $[Re]_{BM}$ of 3380 ppt and 4099 ppt, and in the Peel River the mean $[Re]_{BM}$ = 4473 ± 1842 ppt (n = 4). Much greater variability in $[Re]_{BM}$ is found in the tributaries feeding the Peel River, where $[Re]_{BM}$ varies from 1050 ppt in the West Blackstone River to 321,459 ppt in the Ogilvie River.

In the main channels, the Re concentration in the suspended particulate matter, $[Re]_{SPM}$, ranges from 1805 ppt (Mackenzie River at delta) to 7214 ppt (Arctic Red). On a per catchment basis, the mean $[Re]_{SPM}$ is low in the Liard (2613 ± 295 ppt: n = 4) and the Mackenzie River at Tsiigehtchic (2368 ± 360 ppt: n = 5) and the delta (2708 ± 531 ppt: n = 6) compared with the Arctic Red (7180 ± 70 ppt: n = 2) and Peel rivers (4167 ± 700 ppt: n = 4).

*Organic carbon concentrations.*—The total organic carbon concentration, [OC], of river bed material samples, $[OC]_{BM}$, in the Mackenzie, Liard and Peel catchments has been quantified previously (Hilton and others, 2015). The Mackenzie and Liard have similar values of $[OC]_{BM}$ at 0.16 percent and 0.14 percent, respectively, while the Peel has a higher $[OC]_{BM}$ = 0.75% and the delta has an intermediate value (0.27%). These differences broadly mirror the variability in [Re] values at these locations (see previous section).

River suspended load samples are also similar in terms of their $[OC]_{SPM}$ in the Liard and Mackenzie catchments. We combine data from Hilton and others (2015) with new samples from 2013 and find that the mean $[OC]_{SPM}$ for the Liard is 1.48 ± 0.04% (n = 4), 1.48 ± 0.08% (n = 4) at the Mackenzie (Tsiigehtchic) and 1.60 ± 0.47 % (n = 4) at the delta. In the Peel and Arctic Red river catchments, the $[OC]_{SPM}$ is higher, with mean values of 2.09 ± 0.2% (n = 4) and 2.06 ± 0.22% (n = 2), respectively. The [OC] of river bank samples are, in general, similar to the suspended load at these sites. At the delta, the mean [OC] of 3 bank samples is 1.48 ± 0.87% (n = 3), which is indistinguishable from the suspended load samples. In the Peel, one bank sample is comparable to the suspended load, with a [OC] of 1.4%. A sample that was visibly enriched in woody debris (CAN13-03) has a much higher [OC] of 19.4% (table 4).

*Re to OC ratios.*—The [Re]/[OC] ratio of rocks is a central parameter needed to estimate $CO_2$ emissions using the dissolved Re flux from rivers (Dalai and others, 2002; Petsch, 2014; Hilton and others, 2014). In river sediments from the Mackenzie Basin, the [Re]/[OC] ratio is likely to reflect a mixing between biospheric sources that are comparatively rich in OC and low in Re, and petrogenic OC sources that have lower OC and higher Re concentrations. The former should be enriched in the suspended load (Hilton and others, 2015), while the latter will be more prevalent in river bed materials. This expectation is consistent with the measured [Re]/[OC] values. In the Liard catchment, the mean [Re]/[OC] of the suspended sediments is 1.77 ± 0.22 × $10^{-7}$ g g$^{-1}$ (n = 4), compared to 6.03 × $10^{-7}$ g g$^{-1}$ in the river bed material. In the Mackenzie at Tsiigehtchic, the mean [Re]/[OC] of the suspended sediments is similar

to the Liard at $1.60 \pm 0.28 \times 10^{-7}$ g g$^{-1}$ (n = 5) and the bed material has [Re]/[OC] = $4.67 \times 10^{-7}$ g g$^{-1}$. In the delta, the mean [Re]/[OC] of the suspended sediments is $1.75 \pm 0.24 \times 10^{-7}$ g g$^{-1}$ (n = 6) compared with $3.40 \times 10^{-7}$ g g$^{-1}$ in the bed material. The Peel River sediments have a mean [Re]/[OC] in the suspended load of $2.01 \pm 0.42 \times 10^{-7}$ g g$^{-1}$ (n = 5) and $3.31 \times 10^{-7}$ g g$^{-1}$ in the bed material. The [Re]/[OC] of the Peel River bank material, which is enriched in woody debris, is notably lower than any other sample, $0.36 \times 10^{-7}$ g g$^{-1}$. Altogether, these patterns result in a negative relationship between the [Re]/[OC] of the river sediments and the $^{14}$C activity of their organic matter ($F^{14}$C) (fig. 3A). In this relationship, $F^{14}$C $\sim 0$ would indicate that the sediment is radiocarbon depleted relative to background, as expected for rock organic carbon inputs , whereas an $F^{14}$C $> 0$ suggests an important contribution from biospheric OC that is less than ~55,000 years old. The most $^{14}$C-depleted samples (low $F^{14}$C) have the highest [Re]/[OC] values.

<center>DISCUSSION</center>

To determine whether the Mackenzie River Basin is a source or sink for $CO_2$ as a consequence of erosion and weathering processes, the remaining unknown is the rate of $OC_{petro}$ oxidation (Millot and others, 2003; Calmels and others, 2007; Tank and others, 2012; Hilton and others, 2015). Here, we use Re to provide new insight and quantify weathering fluxes. To do so, we first assess the source of Re derived from rocks using the solid residue of erosion and weathering carried in the suspended load and in the river bed materials, alongside published rock samples (Ross and Bustin, 2009). We then constrain the source of dissolved Re using ion ratios. Having improved constraint on the source and behaviour of Re and its link to $OC_{petro}$, we then seek to quantify weathering fluxes and estimate the $CO_2$ release from $OC_{petro}$ oxidation.

<center>*Insights on the Source of Rhenium*</center>

*River sediments and rocks.*—Sedimentary rocks dominate the Mackenzie River Basin (fig. 1B) and its weathering regime (Millot and others, 2003) and are likely to contain Re-bearing phases in $OC_{petro}$, sulfides and silicate minerals (Dalai and others, 2002; Miller and others, 2011). In an approach adapted from Dalai and others (2002), we normalize Re to major elements sourced from these phases to tease apart their contributions. We use a [Re]/[Na] ratio as a proxy for silicate-derived Re, and assess the Re input from sulfides using a [Re]/[S] ratio. The expectation is that $OC_{petro}$ will have elevated ratios. To help define the ion ratios of the endmembers, we compile published measurements of Re, Na and S concentrations made on specific lithologies and individual minerals (table 5).

For the silicate endmember, we find similar [Re]/[Na] and [Re]/[S] ratios for bulk mantle xenoliths (Bodinier, 1988; Reisberg and Lorand, 1995; Pearson and others, 2004), a spinel-lherzolite (Burton and others, 1999) and basalt (Burton and others, 2002) (table 5). River waters from Iceland draining basaltic rocks also share a similar composition (fig. 4A). We acknowledge that these mafic rock samples and Icelandic river waters may not represent the felsic igneous rocks present in the Mackenzie River Basin (Wheeler and others, 1996). However, published measurements of felsic igneous rocks (Himalayan granite) also have low [Re]/[Na] ratios of <0.002 (Dalai and others, 2002). For the $OC_{petro}$ endmember, a set of organic rich coals from China (Dai and others, 2015) with [OC] >75 percent, highlight the Re enrichment expected for sedimentary organic matter and they have high [Re]/[Na] and [Re]/[S] ratios (fig. 4A). However, we note that organic matter from shales deposited in marine settings may have Re enrichments that are higher than those documented in coals (for example, Selby and Creaser, 2003; Cohen, 2004; Baioumy and others, 2011). Constraining the [Re]/[Na] and [Re]/[S] ratios of sulfides is difficult because Na and S are not necessarily measured alongside Re in these mineral
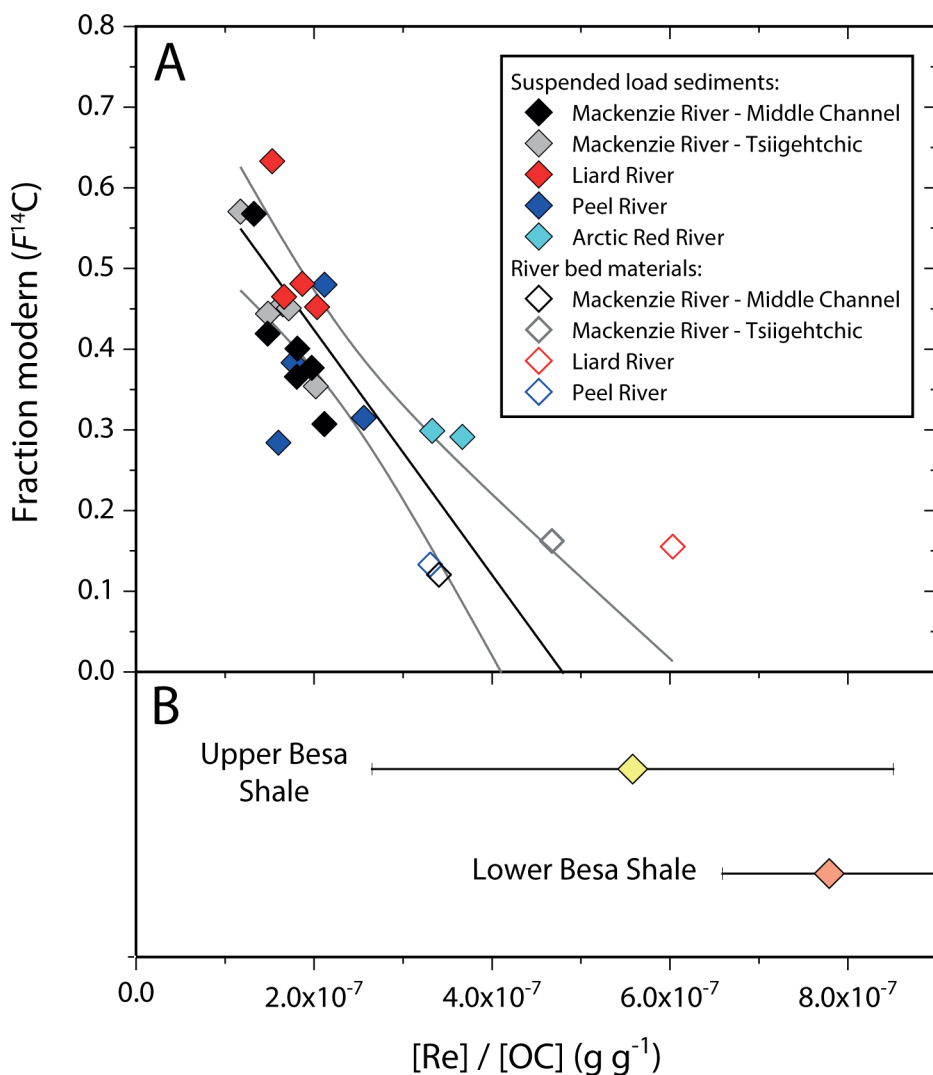
Fig. 3. Rhenium to organic carbon ratios, [Re]/[OC], in Mackenzie River Basin sediments and bedrocks. (A) [Re]/[OC] as a function of the radiocarbon activity of bulk organic matter, reported as $F^{14}C$, for the river suspended load (solid symbols) and river bed materials (open symbols). The black line is a linear regression (Deming) through all the data with gray lines showing the $\pm 95\%$ confidence intervals. Where $F^{14}C = 0$, this provides an indication of the [Re]/[OC$_{petro}$] ratio in each of the catchment. (B) Average [Re]/[OC] ratio for rock samples for the Upper ($n = 8$) and Lower ($n = 7$) Besa Shale (Ross and Bustin, 2009). Whiskers are $\pm 2$ standard errors on the mean.

samples. They are likely to have low [Re]/[S] values, as suggested by Miller and others (2011) who found a median [Re]/[S] ratio in pyrite of $\sim 3 \times 10^{-3}$ pmol/µmol (fig. 4A).

Sedimentary rock samples collected from the lower Liard River basin (Ross and Bustin, 2009) can help to provide local constraint on the source of Re in solid phases. Some of these samples have [Re]/[Na] and [Re]/[S] ratios that approach the values of the organic matter in coal samples from China (fig. 4A). These Liard River basin rock samples also have the highest [OC]/[S] ratios, therefore they seem to represent
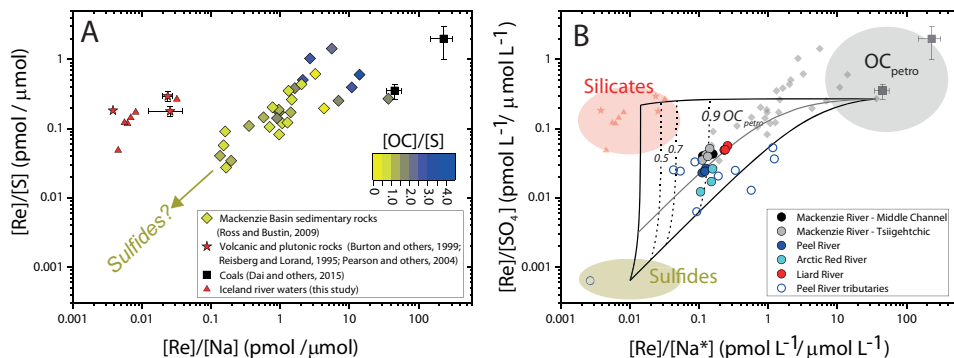
Fig. 4. The source of rhenium in solids and river waters. (A) Rhenium to sodium, [Re]/[Na], and rhenium to sulphur, [Re]/[S], ratios in Chinese coal samples (black squares) and volcanic and plutonic rocks (red stars) (table 5). Red triangles are data from Icelandic rivers draining basalt (table 3) plotted as dissolved ion ratios [Re]/[Na*] and [Re]/[SO$_4$] (where [Na*] is corrected for rainwater inputs). Diamonds are rock samples from the lower Liard river catchment, colored by their organic carbon to total sulfur ratio (Ross and Bustin, 2009) (table 5). Errors are +/− 2SE. (B) [Re]/[Na*] and [Re]/[SO$_4$] ratios for river waters from the Mackenzie basin collected and analyzed for this study (circles), alongside solid samples shown with the same symbol type as part A. Shaded areas indicate the likely source composition of rock-derived organic carbon (OC$_{petro}$), silicate and sulfide endmembers (see discussion in main text). Black lines show the mixing envelope described by these endmembers. Dashed lines are constant proportions of OC$_{petro}$. The gray line is a sulfide:silicate ratio of 0.2:0.8.

an OC$_{petro}$ endmember. Amongst these rock samples, a trend towards lower [Re]/[Na] and [Re]/[S] values broadly tracks a decline in [OC]/[S] ratios, which suggests mixing of OC$_{petro}$ and sulfide derived Re. The pattern in the data are also consistent with a low [Re]/[S] value for pyrite (Miller and others, 2011). Therefore, based on the available samples, it appears that Re in sedimentary rocks from the Mackenzie River Basin mostly comes from the organic and sulfide phases (fig. 4A).

*River waters.*—Previous work has used dissolved ion concentrations alone to examine Re source. For example, a correlation between [Re]$_{diss}$ and [SO$_4$] has been linked to an important role of sulfide minerals (Colodner and others, 1993; Miller and others, 2011). However, dissolved ion concentrations can be strongly moderated by evaporation, dilution and hydrological processes, and correlations between ions may not be associated with a common source (for example, Baronas and others, 2017; Winnick and others, 2017). Indeed, the global [Re]$_{diss}$ data has been shown to be better correlated with [Ca] than with [SO$_4$] (Hilton and others, 2014). Instead of dissolved ion concentrations, the ratios of these ions can provide a useful constraint on source (for example Gaillardet and others, 1999; Tipper and others, 2006).

The [Re]/[Na*] and [Re]/[SO$_4$] values of the Mackenzie River and its tributaries (fig. 4B) are consistent with the sedimentary rocks in the basin (fig. 4A). For the largest rivers (fig. 1A), the samples have similar ratios, suggesting that the main channels integrate dissolved products of weathering and the resulting element ratios are more similar and relatively consistent over time. Tributaries of the Peel River show more variable ion ratios (fig. 4B). For example, the James Creek water sample (CAN13-48) has particularly low [Re]/[Na*] and [Re]/[SO$_4$] values. This Peel River tributary sample has a high [SO$_4$] of 2289 μmol L$^{-1}$, low [HCO$_3$] (95 μmol L$^{-1}$) and a relatively low pH value (6.97) (table 2), suggesting high rates of sulfide oxidation occur here, which are not accompanied by full buffering by dissolution of carbonate minerals (Calmels and others, 2007). We propose that this tributary may help to describe the [Re]/[Na] and [Re]/[S] values of the local sulfide endmember.

The element ratios of the endmembers can be used to estimate the contributions of Re to the dissolved load from silicates, sulfides and organic matter in rocks

(compare Gaillardet and others, 1999; Galy and France Lanord, 1999). This makes the following assumptions: i) the release of Re from the solid endmembers is stoichiometric with the major ions; and ii) the ions behave conservatively. Following the approach of Gaillardet and others (1999) and others, the general form of the mixing equation to determine the relative contribution of the endmembers in figure 4B is given by:

$$\left(\frac{X}{Re}\right)_{diss} = \sum\left(\frac{X}{Re}\right)_i \times \alpha_i(Re) \tag{1}$$

where $i$ refers to the organic matter, sulfide and silicate source reservoirs and $\alpha_i$ is the mixing proportion of Re, with the sum of the $\alpha_i = 1$. The relatively small amount of data preclude an inversion method to estimate the composition of dissolved Re sources at this time.

The mixing space informed by the published measurements of sedimentary rocks from the Mackenzie Basin (fig. 4A), silicate minerals (igneous rocks) and coals, alongside the James Creek water sample as a sulfide endmember, can explain the Re composition at the main stem rivers in the Mackenzie Basin and a large number of the tributary samples (fig. 4B). The mixing model can also provide semi-quantitative constraint on the proportion of $OC_{petro}$. Using equation 1 and the end member compositions shown (fig. 4B) in a forward model, >85 percent of the dissolved Re in the Liard, Peel, Arctic Red and Mackenzie rivers appears to be derived from the $OC_{petro}$ composition (fig. 4B). We note that this percentage is not greatly impacted by modifying the locations of the endmembers within the shaded areas indicated on figure 4B (the percentage varies from ~75 to 90 percent Re derived from $OC_{petro}$) because the mixing space occurs over orders of magnitude variability in the $[Re]/[Na]^*$ and $[Re]/[SO_4]$ values.

In the Mackenzie River Basin, $OC_{petro}$ appears to have a major influence on Re river chemistry relative to silicate and sulfide minerals. A high percentage of $[Re]_{diss}$ contributed by $OC_{petro}$ is consistent with the notion that $[Re]_{diss}$ is primarily hosted in sedimentary organic matter (Selby and Creaser, 2003; Cohen, 2004) and that Re is released during the exposure and oxidation of $OC_{petro}$ (Jaffe and others, 2002). This observation may also relate to the fact that the kinetics of $OC_{petro}$ weathering may be faster than those for silicate weathering (Chang and Berner, 1999; White and Brantley, 2003; Hemingway and others, 2018) and that Re contents are very high in organic matter (Selby and Creaser, 2003; Dai and others, 2015). However, it is important to recognise that our endmember mixing model (fig. 4B) has limited constraint on the exact $[Re]/[Na^*]$ and $[Re]/[S]$ values of the Re sources and their spatial variability, with the sulfide endmember in particular not being well constrained. A potential caveat relates to sulfate cycling in river catchments, which can drive S to be non-conservative; particularly when it is linked to secondary sulfide precipitation (Turchyn and others, 2013; Torres and others, 2017). Sequential extractions of solid samples may provide constraint on the composition of each mineral phase, and an analysis of Re isotopes may help in characterising organic and silicate host phases (Miller and others, 2015). Nevertheless, the ion ratios (fig. 4B) are consistent with the notion that sedimentary organic matter is a key component in the surficial cycle of Re (Colodner and others, 1993; Jaffe and others, 2002; Miller and others, 2011).

*Estimates of CO$_2$ Fluxes via OC$_{petro}$ Oxidation*

To estimate $CO_2$ emissions by $OC_{petro}$ oxidation, the dissolved Re flux can be combined with the $[Re]/[OC]$ of the bedrocks undergoing weathering (Jaffe and others, 2002; Hilton and others, 2014; Petsch, 2014). Here, we refine this approach by following a similar method as Dalai and others (2002), whereby we use dissolved ion ratios to constrain the fraction of dissolved Re derived from $OC_{petro}$ weathering (see

the *Insights on the Source of Rhenium* section, fig. 4). Long-term average annual $Q_w$ from gauging stations account for runoff variability that has been monitored over several decades and these values are combined with the average $[Re]_{diss}$ measurements and their variability (see the *Dissolved Rhenium Concentration and Flux* section). Annual Re fluxes are estimated to be $250 \pm 31 \times 10^3$ g yr$^{-1}$, $684 \pm 48 \times 10^3$ g yr$^{-1}$, $60 \pm 15 \times 10^3$ g yr$^{-1}$ and $13 \pm 3.6 \times 10^3$ g yr$^{-1}$, for the Liard, the Mackenzie at Tsiigehtchic, the Peel, and the Arctic Red catchments, respectively.

In order to constrain the $[Re]/[OC]$ ratio of the rocks in these catchments, we consider the $[Re]/[OC]$ ratios of the river suspended sediments and the bed materials together with radiocarbon measurements on the organic matter (Hilton and others, 2015), reported using the "Fraction Modern" ($F^{14}C$) notation (Reimer and others, 2004). The petrogenic OC is defined as having $F^{14}C \sim 0$, because it is fully $^{14}C$-depleted relative to the analytical background. We find that the river bed materials could offer a good indication of the $[Re]/[OC]$ of the source rock, as they have low $^{14}C$ content (low $F^{14}C$). Nevertheless, because $F^{14}C$ values do exceed 0, the river bed materials must contain some biospheric organic carbon (Hilton and others, 2015) incorporated as the sediments were weathered and eroded upstream. The contribution of biospheric OC is highest in the suspended sediments, which have higher $F^{14}C$. The $[Re]/[OC]$ of the suspended load samples is also lower than that of the bed materials (fig. 3A), with input of Re-poor organic-rich material in these samples. The $[Re]/[OC]$ ratio of a wood rich sample in the Peel River is $3.58 \times 10^{-8}$ g g$^{-1}$, supporting the idea that the patterns in the data can be explained by the mixing of OC sources – high $[Re]/[OC]$ in sedimentary rocks, and low $[Re]/[OC]$ from the terrestrial biosphere. Organic carbon-rich surface soil litters from other locations, such as Taiwan and New Zealand, have similar low $[Re]/[OC]$ ratios; these are $1.3 \times 10^{-9}$ and $9.5 \times 10^{-9}$ g g$^{-1}$, respectively (Hilton and others, 2014; Horan and others, 2017).

By fitting a linear regression through the $F^{14}C$ values versus $[Re]/[OC]$ for both river bed materials and suspended loads, we can constrain the average $[Re]/[OC_{petro}]$ composition of the sedimentary rocks in the basin. This approach yields an intercept on the $[Re]/[OC]$ axis that broadly reflects the $[Re]/[OC]$ composition of the source rock when $F^{14}C = 0$ (fig. 3A), assuming that the river bed materials have had minimal $OC_{petro}$ oxidation and contain most Re in the organic phases. The combined linear regression for all catchments indicates a $[Re]/[OC]$ ratio of $4.8 \pm 0.9 \times 10^{-7}$ g g$^{-1}$ ($\pm 95\%$ confidence) (fig. 3A). This value agrees with published mean values of bedrocks from the Besa Shale collected from the Liard sub-catchment (fig. 3B) (Ross and Bustin, 2009). With more data, it may be possible to take this approach for each sampling location. The intercept on the $F^{14}C$ axis and its uncertainty provides an indication of the $^{14}C$ activity of the biosphere and with $F^{14}C$ values of $\sim 0.5$ to $0.7$ it is consistent with the erosion of aged soil organic carbon in the Mackenzie River Basin (Hilton and others, 2015).

Together, the dissolved Re yield ($J_{Re}$, g km$^{-2}$ yr$^{-1}$) and the $[OC]/[Re]$ ratio of sedimentary rocks (g g$^{-1}$) allow us to make an estimate of the $OC_{petro}$ $CO_2$ oxidation yield, $J_{OCpetro-ox}$ (gC km$^{-2}$ yr$^{-1}$) by $OC_{petro}$ oxidation:

$$J_{OCpetro-ox} = J_{Re} \times ([OC]/[Re])_{petro} \times f_C \times (1 - f_{graphite}) \qquad (2)$$

The term $f_C$ reflects the proportion of the dissolved Re flux derived from $OC_{petro}$, and it is estimated here from the mixing analysis (see previous section, fig. 4B). It is included so that non-$OC_{petro}$ sources of Re in the dissolved load are accounted for and the resultant $CO_2$ fluxes are less likely to be overestimated. The forward model based on the end member compositions described in previous section (fig. 4B) suggest $>85$ percent of the Re in the main rivers is derived from $OC_{petro}$. However, given the uncertainty on the end member compositions, we use a range of $f_c$ from $0.75$ to $0.90$.

The term $f_{graphite}$ accounts for the fraction of graphitic carbon in the rocks that may be resilient to oxidation (Galy and others, 2008). High grade metamorphic rocks are not as common in the mountain uplands of the Mackenzie Basin (figs. 1B and 1C), compared to Taiwan and the Southern Alps (Beyssac and others, 2016) where the Re proxy has been recently applied (Hilton and others, 2014; Horan and others, 2017). Therefore, we vary the fraction of $OC_{petro}$ as graphite from 0 to 0.2 in this analysis. The $CO_2$ oxidation flux, $J_{OCpetro-ox}$, is then calculated and a Monte Carlo simulation is used to account for these uncertainties following the approach of Horan and others (2017).

In the Mackenzie River catchment, based on $[Re]_{diss}$ fluxes at Tsiigehtchic we quantify a $CO_2$ yield from $OC_{petro}$ oxidation to be 0.45 $^{+0.19}/_{-0.11}$ tC km$^{-2}$ yr$^{-1}$, or 3.8 $^{+1.5}/_{-0.9} \times 10^4$ moles km$^{-2}$ yr$^{-1}$ (figs. 1A and 2). In the Peel, Arctic Red and Liard catchments, we find $CO_2$ yields from $OC_{petro}$ oxidation are higher, at 0.94 $^{+0.41}/_{-0.26}$ tC km$^{-2}$ yr$^{-1}$, 0.78 $^{+0.35}/_{-0.21}$ tC km$^{-2}$ yr$^{-1}$ and 1.01 $^{+0.42}/_{-0.25}$ tC km$^{-2}$ yr$^{-1}$, respectively (table 6). For comparison, the river flux of un-weathered $OC_{petro}$ in the solid load is ~0.6 $^{+0.2}/_{-0.2}$ tC km$^{-2}$ yr$^{-1}$ in the Mackenzie River (Hilton and others, 2015). This suggests that oxidative weathering makes up ~40 percent of the total $OC_{petro}$ denudation in the Mackenzie River, which is higher than more erosive catchments in Taiwan (Hilton and others, 2014).

To explain the differences in weathering yields between the catchments, we consider how the physical erosion rates vary between the catchments. Physical erosion is thought to enhance the rate of oxidative weathering of organic carbon in rocks at the river catchment scale (Hilton and others, 2014), therefore we might expect $[Re]_{diss}$ and associated $CO_2$ fluxes in the Mackenzie River Basin to be governed by this parameter. We use published sediment yields (t km$^{-2}$ yr$^{-1}$) as a measure of physical erosion rate. In the Mackenzie River catchment, sediment yields are 124 t km$^{-2}$ yr$^{-1}$, while the Peel, Liard and Arctic Red catchments experience sediment yields of 295 t km$^{-2}$ yr$^{-1}$, 149 t km$^{-2}$ yr$^{-1}$ and 392 t km$^{-2}$ yr$^{-1}$, respectively (Carson and others, 1998, 1999). The Peel and Liard rivers have the highest sediment yields, dissolved Re yields and estimated $OC_{petro}$ oxidation yields. The sediment yields are 10 to 100 times lower than those recorded in the mountain belts of New Zealand and Taiwan, and the Re yields and $OC_{petro}$ oxidation rates are also lower by a similar magnitude in the Mackenzie River Basin (table 6) (Hilton and others, 2014; Horan and others, 2017). Altogether, the data from the Mackenzie River Basin strengthen the hypothesis that more rapid erosion of sedimentary rocks can increase $CO_2$ emissions by $OC_{petro}$ oxidation (Hilton and others, 2014).

### *The Net CO$_2$ Budget of the Mackenzie River Catchment During Weathering and Erosion*

Examining the transfer of Re across the Mackenzie River Basin has allowed us to assess the rate and controls on $OC_{petro}$ oxidation while also estimating, for the first time, the associated $CO_2$ release. In the Mackenzie River catchment, we are able to combine our estimates of $CO_2$ flux from $OC_{petro}$ oxidation ($J_{OCpetro-ox} = 0.45$ $^{+0.19}/_{-0.11}$ tC km$^{-2}$ yr$^{-1}$) with pre-existing data on biospheric organic carbon burial rates and silicate and carbonate weathering rates to calculate the net geochemical carbon budget. Petrogenic carbon sources (rock-organic matter and carbonate minerals) must be differentiated from atmospheric carbon to understand how the key transfers occur between the atmosphere, sedimentary rocks exposed to weathering and erosion and long term sedimentary storage (fig. 5).

The silicate weathering $CO_2$ consumption during weathering is ~0.52 tC km$^{-2}$ yr$^{-1}$ and when coupled to carbonate precipitation equates to long term sink of $J_{sil-CO2} \sim 0.26$ tC km$^{-2}$ yr$^{-1}$ (Gaillardet and others, 1999). The $CO_2$ release by sulfuric acid driven carbonate weathering is $J_{carb-sulf} \sim 0.71$ tC km$^{-2}$ yr$^{-1}$ (Calmels and others, 2007). The drawdown of atmospheric $CO_2$ by carbonate weathering by carbonic acid

TABLE 6

*Estimates of $OC_{petro}$ oxidation for the Mackenzie River Basin*

| River catchment | Area (km$^2$) | Runoff (mm yr$^{-1}$) | Discharge (m$^3$ s$^{-1}$) | Ref. | Suspended sediment yield (t km$^{-2}$ yr$^{-1}$) | Ref. | [Re]$_{diss}$ average (ppt) | ±SE | [Re]/[C]* (g/g) | ±SE | Ref. | CO$_2$ flux** (t km$^{-2}$ yr$^{-1}$) | + error | - error |
|---|---|---|---|---|---|---|---|---|---|---|---|---|---|---|
| Mackenzie | 1680000 | 134 | 7156 | Environment Canada long-term discharges (1972–2015) | 124 | Carson 1998 | 3.03 | 0.11 | 4.8x10$^{-7}$ | 0.9x10$^{-07}$ | This study | 0.45 | 0.19 | 0.11 |
| Peel | 70600 | 240 | 538 | Environment Canada long-term discharges (1969–2015) | 295 | Carson 1998 | 3.56 | 0.44 | 4.8x10$^{-7}$ | 0.9x10$^{-07}$ | This study | 0.94 | 0.41 | 0.26 |
| Arctic Red | 18600 | 211 | 124 | Environment Canada long-term discharges (1968–2015) | 392 | Carson 1998 | 3.39 | 0.46 | 4.8x10$^{-7}$ | 0.9x10$^{-07}$ | This study | 0.78 | 0.35 | 0.21 |
| Liard | 275000 | 223 | 1944 | Environment Canada long-term discharges (1972–2015) | 149 | Carson 1998 | 4.07 | 0.25 | 4.8x10$^{-7}$ | 0.9x10$^{-07}$ | This study | 1.01 | 0.42 | 0.25 |

*From figure 3, the intercept at $F^{14}C = 0$.
**This calculation uses equation 1 and corrects for Re source and takes account of the fraction of OC$_{petro}$ that may be present as graphite and less susceptible to oxidation.
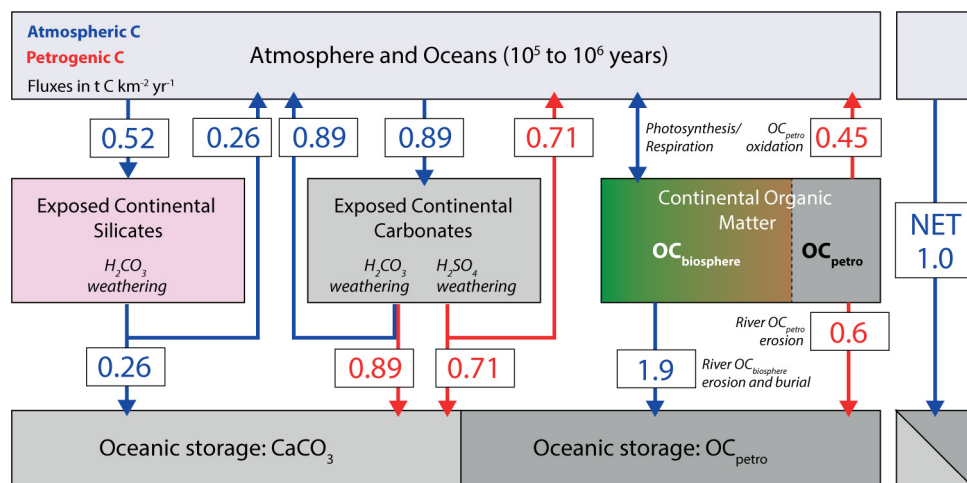
Fig. 5. Geochemical carbon budget of the Mackenzie River Basin during weathering and erosion. A distinction is made between carbon transfers (in $tC \, km^{-2} \, yr^{-1}$) derived from atmospheric C (blue) versus those from petrogenic C (red). The latter comprises both rock-derived organic carbon ($OC_{petro}$) and carbonate minerals ($CaCO_3$). Carbon is tracked from the atmosphere and ocean reservoir through exposed sedimentary rocks (silicates and carbonates) and organic matter, down into sedimentary storage in long-lived ocean sediments as $CaCO_3$ or $OC_{petro}$. $OC_{petro}$ oxidation yield is from this study. Silicate and carbonate weathering fluxes are from Gaillardet and others (1999) and Calmels and others (2007) and erosional organic carbon fluxes are from Hilton and others (2015). The net carbon balance consumes atmospheric $CO_2$.

is $\sim 0.89 \, tC \, km^{-2} \, yr^{-1}$, but this is often considered to be $CO_2$ neutral over timescales of $10^3 - 10^6$ years when coupled to carbonate mineral precipitation (Gaillardet and othes, 1999) so is not included in the calculation. Erosion of biospheric OC from vegetation and soils drives a $CO_2$ sink over millennial timescales, and assuming a burial efficiency of 65 percent corresponds to $J_{OCbio-burial} \sim 1.9 \, tC \, km^{-2} \, yr^{-1}$ (Hilton and others, 2015). When taken together with our new constraints on $OC_{petro}$ oxidation ($J_{OCpetro-ox}$), the net transfer of $CO_2$ from the atmosphere to the lithosphere during erosion and weathering, $J_{net}$, can be calculated as the sum of the organic and inorganic carbon cycles as follows:

$$J_{net} = (J_{OCbio-burial} - J_{OCpetro-ox}) + (J_{sil-CO2} - J_{carb-sulf}) \qquad (3)$$

The published data and the new constraints on $OC_{petro}$ oxidation provided here suggest that the Mackenzie River catchment has a net geochemical $CO_2$ budget that equates to a transfer of $\sim 1 \, tC \, km^{-2} \, yr^{-1}$ of carbon from the atmosphere to the lithosphere. This transfer is relevant to the carbon cycle over timescales of $10^3$ to $10^6$ years (fig. 5).

### Wider Implications for the Global Carbon Cycle

Estimates of $CO_2$ flux from $OC_{petro}$ oxidation are limited globally. Therefore, our understanding of the net geochemical carbon balance in catchments during weathering and erosion remains tentative. Current carbon flux estimates for non-glaciated mountainous regions in Taiwan (Hilton and others, 2014; Hemingway and others, 2018) and New Zealand (Horan and others, 2017) appear to trend toward net sinks of atmospheric $CO_2$. Although $OC_{petro}$ oxidation counterbalances silicate weathering in each of these sites, the drawdown of $CO_2$ by biospheric organic carbon erosion tends to control the net carbon balance. This is also what we observe in the Mackenzie River

Basin, where high rates of erosion of OC from soils creates a significant carbon sink (fig. 5). This is an important observation, as many numerical models of the long-term geochemical carbon cycle forced by weathering and erosion do not presently consider these processes (see for example, Carretier and others, 2018).

The extent to which the net $CO_2$ balance during weathering and erosion may change over time in large river basins is not well known. Silicate weathering rates should be sensitive to changes in climate, including temperature and hydrological parameters (West and others, 2005; Maher and Chamberlain, 2014). Similarly, the rates of biospheric OC burial by erosion may be regulated by climate through hydrological processes (Hilton, 2017). For the $CO_2$ sources from oxidation of sedimentary rocks, mountain catchments subject to glaciation appear to have greater carbonate dissolution by sulphuric acid (Torres and others, 2017a) and more than double the $CO_2$ emissions by $OC_{petro}$ oxidation (Horan and others, 2017).

If we consider that at the Last Glacial Maximum vast areas of the Mackenzie River Basin were glaciated, the net geochemical carbon balance could have looked very different. Mountain glaciation of sedimentary rocks (figs. 1A and 1B) could have strengthened the $CO_2$ emissions from oxidative weathering, while lower organic carbon stocks in the landscape and lower temperatures could simultaneously weaken the $CO_2$ drawdown by biospheric OC burial and silicate weathering. This region may have acted as a $CO_2$ source during colder global climate conditions, rather than as a $CO_2$ sink during the present interglacial (fig. 5). Based on these inferences, it is now essential to consider how the inorganic and organic geochemical carbon cycles act in tandem in large river basins to dampen warming and cooling trends at Earth's surface by moderating atmospheric $CO_2$ concentrations.

<div align="center">CONCLUSION</div>

Rhenium concentrations and fluxes are used to quantify the rates and patterns of oxidative weathering of rock-derived organic matter and the associated $CO_2$ emissions to the atmosphere in the Mackenzie River Basin. River water and sediments collected from 2009–2013 at sites on the main Mackenzie River and its tributaries are used to assess spatial and temporal changes in chemical weathering and Re mobility. In the dissolved load, we examine Re source (from silicate minerals, sulfides and $OC_{petro}$) using [Re]/[Na] and [Re]/[$SO_4$] ratios. Based on endmember compositions from a literature compilation and published data from sedimentary rocks in the Mackenzie River Basin, we estimate that >85 percent of the dissolved Re is derived from $OC_{petro}$ at the main channel sampling sites. Dissolved Re flux measurements are used together with estimates of bedrock [Re]/[OC] to quantify $CO_2$ release by $OC_{petro}$ oxidation. The [Re]/[OC] of the un-weathered source rock is constrained using [Re]/[OC] and $^{14}$C activity of organic matter in river suspended sediments and bed materials. The uncertainties on the $CO_2$ flux reflect the potential for non-$OC_{petro}$ sources of dissolved Re and the presence of graphitic carbon that is less susceptible to oxidation, but they are assessed using a Monte Carlo Simulation.

We conclude that $OC_{petro}$ oxidation is a significant source of $CO_2$ to the atmosphere in the Mackenzie River Basin, of 0.45 $^{+0.19}/_{-0.11}$ tC km$^{-2}$ yr$^{-1}$. This is higher than the $CO_2$ consumption by silicate weathering. We produce the first geochemical carbon budget of a large river basin, assessing the $CO_2$ emission from $OC_{petro}$ oxidation, alongside drawdown of $CO_2$ by silicate weathering and erosion and burial of terrestrial biospheric OC, and $CO_2$ release from carbonate dissolution by sulphuric acid. At present, erosion and weathering in the Mackenzie River catchment drive organic and inorganic cycles to combine to form a carbon sink of ~1 tC km$^{-2}$ yr$^{-1}$. The potency of this sink mainly depends on the ratio between $OC_{petro}$ oxidation and biospheric carbon erosion and burial. We postulate that this may not have been

constant over glacial–interglacial cycles, which will have impacted the net $CO_2$ budget of this large river basin.

## ACKNOWLEDGMENTS

## REFERENCES

Baioumy, H. M., Eglinton, L. B., and Peucker-Ehrenbrink, B., 2011, Rhenium–osmium isotope and platinum group element systematics of marine vs. non-marine organic-rich sediments and coals from Egypt: Chemical Geology, v. 285, n. 1–4, p. 70–81, https://doi.org/10.1016/j.chemgeo.2011.02.026

Baronas, J. J., Torres, M. A., Clark, K. E., and West, A. J., 2017, Mixing as a driver of temporal variations in river hydrochemistry: 2. Major and trace element concentration dynamics in the Andes-Amazon transition: Water Resources Research, v. 53, n. 4, p. 3120–3145, https://doi.org/10.1002/2016WR019729

Beaulieu, E., Goddéris, Y., Labat, D., Roelandt, C., Calmels, D., and Gaillardet, J., 2011, Modeling of water-rock interaction in the Mackenzie basin: Competition between sulfuric and carbonic acids: Chemical Geology, v. 289, n. 1–2, p. 114–123, https://doi.org/10.1016/j.chemgeo.2011.07.020

Berner, R. A., 1982, Burial of organic-carbon and pyrite sulfur in the modern ocean – Its geochemical and environmental significance: American Journal of Science, v. 282, n. 4, p. 451–473, https://doi.org/10.2475/ajs.282.4.451

Berner, R. A., and Caldeira, K., 1997, The need for mass balance and feedback in the geochemical carbon cycle: Geology, v. 25, n. 10, p. 955–956, https://doi.org/10.1130/0091-7613(1997)025<0955:TNFMBA>2.3.CO;2

Berner, R. A., and Canfield, D. E., 1989, A new model for atmospheric oxygen over Phanerozoic time: American Journal of Science, v. 289, n. 4, p. 333–361, https://doi.org/10.2475/ajs.289.4.333

Berner, R. A., and Maasch, K. A., 1996, Chemical weathering and controls on atmospheric $O_2$ and $CO_2$: Fundamental principles were enunciated by J.J. Ebelmen in 1845: Geochimica et Cosmochimica Acta, v. 60, n. 9, p. 1633–1637, https://doi.org/10.1016/0016-7037(96)00104-4

Beyssac, O., Cox, S. C., Vry, J., and Herman, F., 2016, Peak metamorphic temperature and thermal history of the Southern Alps (New Zealand): Tectonophysics, v. 676, p. 229–249, https://doi.org/10.1016/j.tecto.2015.12.024

Bodinier, J. L., 1988, Geochemistry and petrogenesis of the Lanzo peridotite body, western Alps: Tectonophysics, v. 149, n. 1–2, p. 67–88, https://doi.org/10.1016/0040-1951(88)90119-9

Bolton, E. W., Berner, R. A., and Petsch, S. T., 2006, The weathering of sedimentary organic matter as a control on atmospheric $O_2$: II. Theoretical modeling: American Journal of Science, v. 306, n. 8, p. 575–615, https://doi.org/10.2475/08.2006.01

Bouchez, J., Beyssac, O., Galy, V., Gaillardet, J., France-Lanord, C., Maurice, L., and Moreira-Turcq, P., 2010, Oxidation of petrogenic organic carbon in the Amazon floodplain as a source of atmospheric $CO_2$: Geology, v. 38, n. 3, p. 255–258, https://doi.org/10.1130/G30608.1

Bouchez, J., Galy, V., Hilton, R. G., Gaillardet, J., Moreira-Turcq, P., Perez, M. A., France-Lanord, C., and Maurice, L., 2014, Source, transport and fluxes of Amazon River particulate organic carbon: Insights from river sediment depth-profiles: Geochimica et Cosmochimica Acta, v. 133, p. 280–298, https://doi.org/10.1016/j.gca.2014.02.032

Burton, K.W., Schiano, P., Birck, J. L., and Allegre, C. J., 1999, Osmium isotope disequilibrium between mantle minerals in a spinel-lherzolite: Earth and Planetary Science Letters, v. 172, p. 311–322, https://doi.org/10.1016/S0012-821X(99)00207-1

Burton, K. W., Gannoun, A., Birck, J.-L., Allègre, C. J., Schiano, P., Clocchiatti, R., and Alard, O., 2002, The compatibility of rhenium and osmium in natural olivine and their behaviour during mantle melting and basalt genesis: Earth and Planetary Science Letters, v. 198, n. 1–2, p. 63–76, https://doi.org/10.1016/S0012-821X(02)00518-6

Calmels, D., Gaillardet, J., Brenot, A., and France-Lanord, C., 2007, Sustained sulfide oxidation by physical erosion processes in the Mackenzie River basin: Climatic perspectives: Geology, v. 35, n. 11, p. 1003–1006, https://doi.org/10.1130/G24132A.1

Carretier, S., Goddéris, Y., Martinez, J., Reich, M., and Martinod, P., 2018, Colluvial deposits as a possible weathering reservoir in uplifting mountains: Earth Surface Dynamics, v. 6, p. 217–237, https://doi.org/10.5194/esurf-6-217-2018

Carson, M. A., Jasper, J. N., and Conly, F. M., 1998, Magnitude and Sources of Sediment Input to the Mackenzie Delta, Northwest Territories, 1974-94: Arctic, v. 51, n. 2, p. 116–124, https://doi.org/10.14430/arctic1053

Carson, M. A., Conly, F. M., and Jasper, J. N., 1999, Riverine sediment balance of the Mackenzie Delta, Northwest Territories, Canada: Hydrological Processes, v. 13, n. 16, p. 2499–2518, https://doi.org/10.1002/(SICI)1099-1085(199911)13:16<2499::AID-HYP937>3.3.CO;2-9

Chang, S. B., and Berner, R. A., 1999, Coal weathering and the geochemical carbon cycle: Geochimica et Cosmochimica Acta, v. 63, n. 19–20, p. 3301–3310, https://doi.org/10.1016/S0016-7037(99)00252-5

Cohen, A. S., 2004, The rhenium-osmium isotope system: Applications to geochronological and palaeoenvironmental problems: Journal of the Geological Society, London, v. 161, n. 4, p. 729–734, https://doi.org/10.1144/0016-764903-084

Colodner, D., Sachs, J., Ravizza, G., Turekian, K., Edmond, J., and Boyle, E., 1993a, The geochemical cycle of rhenium: A reconnaissance: Earth and Planetary Science Letters, v. 117, n. 1–2, p. 205–221, https://doi.org/10.1016/0012-821X(93)90127-U

Cumming, V. M., Poulton, S. W., Rooney, A. D., and Selby, D., 2013, Anoxia in the terrestrial environment during the late Mesoproterozoic: Geology, v. 41, n. 5, p. 583–586, https://doi.org/10.1130/G34299.1

Dai, S. F., Seredin, V. V, Ward, C. R., Hower, J. C., Xing, Y. W., Zhang, W. G., Song, W. J., and Wang, P. P., 2015, Enrichment of U-Se-Mo-Re-V in coals preserved within marine carbonate successions: Geochemical and mineralogical data from the Late Permian Guiding Coalfield, Guizhou, China: Mineralium Deposita, v. 50, n. 2, p. 159–186, https://doi.org/10.1007/s00126-014-0528-1

Dalai, T. K., Singh, S. K., Trivedi, J. R., and Krishnaswami, S., 2002, Dissolved rhenium in the Yamuna River System and the Ganga in the Himalaya: Role of black shale weathering on the budgets of Re, Os, and U in rivers and CO$_2$ in the atmosphere: Geochimica et Cosmochimica Acta, v. 66, n. 1, p. 29–43, https://doi.org/10.1016/S0016-7037(01)00747-5

Dellinger, M., ms, 2013, Apport des isotopes du lithium et des éléments alcalins à la compréhension des processus d'altération chimique et de recyclage sédimentaire: Paris, France, Institut de Physique du Globe de Paris, Ph. D. thesis.

Dellinger, M., Gaillardet, J., Bouchez, J., Calmels, D., Galy, V., Hilton, R. G., Louvat, P., and France-Lanord, C., 2014. Lithium isotopes in large rivers reveal the cannibalistic nature of modern continental weathering and erosion: Earth and Planetary Science Letters, v. 401, p. 359–372, https://doi.org/10.1016/j.epsl.2014.05.061

Ebelmen, J. J., 1845, Sur les produits de la décomposition desespèces minérales de la famille des silicates: Annales des Mines, v. 7, p. 3–66.

Emberson, R., Hovius, N., Galy, A., and Marc, O., 2016, Chemical weathering in active mountain belts controlled by stochastic bedrock landsliding: Nature Geoscience, v. 9, p. 42–45, https://doi.org/10.1038/ngeo2600

Environment Canada. Water Survey of Canada. <https://www.canada.ca/en/environment-climate-change/services/water-overview/quantity/monitoring/survey.html> (accessed 5.10.17).

Gaillardet, J., Dupré, B., Louvat, P., and Allègre, C. J., 1999, Global silicate weathering and CO$_2$ consumption rates deduced from the chemistry of large rivers: Chemical Geology, v. 159, n. 1–4, p. 3–30, https://doi.org/10.1016/S0009-2541(99)00031-5

Galy, A., and France-Lanord, C., 1999, Weathering processes in the Ganges-Brahmaputra basin and the riverine alkalinity budget: Chemical Geology, v. 159, n. 1–4, p. 31–60, https://doi.org/10.1016/S0009-2541(99)00033-9

Galy, V., Bouchez, J., and France-Lanord, C., 2007, Determination of total organic carbon content and $\delta^{13}$C in carbonate-rich detrital sediments: Geostandards and Geoanalytical Research, v. 31, n. 3, p. 199–207, https://doi.org/10.1111/j.1751-908X.2007.00864.x

Galy, V., Beyssac, O., France-Lanord, C., and Eglinton, T., 2008, Recycling of Graphite During Himalayan Erosion: A Geological Stabilization of Carbon in the Crust: Science, v. 322, n. 5903, p. 943–945, https://doi.org/10.1126/science.1161408

Gramlich, J. W., Murphy, T. J., Garner, E. L., and Shields, W. R., 1973, Absolute isotopic abundance ratio and atomic weight of a reference sample of rhenium: Journal of Research of the National Bureau of Standards- Section A Physics and Chemistry, v. 77A, n. 6, p. 691–698, https://doi.org/10.6028/jres.077A.040

Hayes, J. M., and Waldbauer, J. R., 2006, The carbon cycle and associated redox processes through time: Philosophical Transactions of the Royal Society B: Biological Sciences, v. 361, n. 1470, p. 931–950, https://doi.org/10.1098/rstb.2006.1840

Hemingway, J. D., Hilton, R. G., Hovius, N., Eglinton, T. I., Haghipour, N., Wacker, L., Chen, M.-C., and Galy, V. V., 2018, Microbial oxidation of lithospheric organic carbon in rapidly eroding tropical mountain soils: Science, v. 360, n. 6385, p. 209–212, https://doi.org/10.1126/science.aao6463

Hilton, R. G., 2017, Climate regulates the erosional carbon export from the terrestrial biosphere: Geomorphology, v. 277, p. 118–132, https://doi.org/10.1016/j.geomorph.2016.03.028

Hilton, R. G., Gaillardet, J., Calmels, D., and Birck, J.-L., 2014, Geological respiration of a mountain belt revealed by the trace element rhenium: Earth and Planetary Science Letters, v. 403, p. 27–36, https://doi.org/10.1016/j.epsl.2014.06.021

Hilton, R. G., Galy, V., Gaillardet, J., Dellinger, M., Bryant, C., O'Regan, M., Grocke, D. R., Coxall, H.,

Bouchez, J., and Calmels, D., 2015, Erosion of organic carbon in the Arctic as a geological carbon dioxide sink: Nature, v. 524, p. 84–87, https://doi.org/10.1038/nature14653

Holmes, R. M., McClelland, J. W., Peterson, B. J., Shiklomanov, I. A., Shiklomanov, A. I., Zhulidov, A. V., Gordeev, V. V., and Bobrovitskaya, N. N., 2002, A circumpolar perspective on fluvial sediment flux to the Arctic ocean: Global Biogeochemical Cycles, v. 16, n. 4, 45-1-45–14, https://doi.org/10.1029/2001GB001849

Horan, K., Hilton, R. G., Selby, D., Ottley, C. J., Gröcke, D. R., Hicks, M., and Burton, K. W., 2017, Mountain glaciation drives rapid oxidation of rock-bound organic carbon: Science Advances, 3, n. 10, https://doi.org/10.1126/sciadv.1701107

Huh, Y., Birck, J. L., and Allègre, C. J., 2004, Osmiurn isotope geochemistry in the Mackenzie River basin: Earth and Planetary Science Letters, v. 222, n. 1, p. 115–129, https://doi.org/10.1016/j.epsl.2004.02.026

Jaffe, L. A., Peucker-Ehrenbrink, B., and Petsch, S. T., 2002, Mobility of rhenium, platinum group elements and organic carbon during black shale weathering: Earth and Planetary Science Letters, v. 198, n. 3–4, p. 339–353, https://doi.org/10.1016/S0012-821X(02)00526-5

Johnston, D. T., Macdonald, F. A., Gill, B. C., Hoffman, P. F., and Schrag, D. P., 2012, Uncovering the Neoproterozoic carbon cycle: Nature, v. 483, p. 320, https://doi.org/10.1038/nature10854

Larsen, I. J., Almond, P. C., Eger, A., Stone, J. O., Montgomery, D. R., and Malcolm, B., 2014, Rapid Soil Production and Weathering in the Southern Alps, New Zealand: Science, v. 343, p. 637–640, https://doi.org/10.1126/science.1244908

Macdonald, R. W., Solomon, S. M., Cranston, R. E., Welch, H. E., Yunker, M. B., and Gobeil, C., 1998, A sediment and organic carbon budget for the Canadian beaufort shelf: Marine Geology, v. 144, n. 4, p. 255–273, https://doi.org/10.1016/S0025-3227(97)00106-0

Maher, K., 2011, The role of fluid residence time and topographic scales in determining chemical fluxes from landscapes: Earth and Planetary Science Letters, v. 312, n. 1–2, p. 48–58, https://doi.org/10.1016/j.epsl.2011.09.040

Maher, K., and Chamberlain, C. P., 2014, Hydrologic Regulation of Chemical Weathering and the Geologic Carbon Cycle: Science, v. 343, n. 6178, p. 1502–1504, https://doi.org/10.1126/science.1250770

Marty, B., and Tolstikhin, I. N., 1998, $CO_2$ fluxes from mid-ocean ridges, arcs and plumes: Chemical Geology, v. 145, n. 3–4, p. 233–248, https://doi.org/10.1016/S0009-2541(97)00145-9

McClelland, J. W., Holmes, R. M., Peterson, B. J., Raymond, P. A., Striegl, R. G., Zhulidov, A. V., Zimov, S. A., Zimov, N., Tank, S. E., Spencer, R. G. M., Staples, R., Gurtovaya, T. Y., and Griffin, C. G., 2016, Particulate organic carbon and nitrogen export from major Arctic rivers: Global Biogeochemical Cycles, v. 30, n. 5, p. 629–643, https://doi.org/10.1002/2015GB005351

Meisel, T., and Moser, J., 2004, Platinum-Group Element and Rhenium Concentrations in Low Abundance Reference Materials: Geostandards and Geoanalytical Research, v. 28, n. 2, p. 233–250., https://doi.org/10.1111/j.1751-908X.2004.tb00740.x

Meybeck, M., 1987, Global chemical weathering of surficial rocks estimated from river dissolved loads: American Journal of Science, v. 287, n. 5, p. 401–428, https://doi.org/10.2475/ajs.287.5.401

Miller, C. A., Peucker-Ehrenbrink, B., Walker, B. D., and Marcantonio, F., 2011, Re-assessing the surface cycling of molybdenum and rhenium: Geochimica et Cosmochimica Acta, v. 75, n. 22, p. 7146–7179, https://doi.org/10.1016/j.gca.2011.09.005

Miller, C. A., Peucker-Ehrenbrink, B., and Schauble, E. A., 2015, Theoretical modeling of rhenium isotope fractionation, natural variations across a black shale weathering profile, and potential as a paleoredox proxy: Earth and Planetary Science Letters, v. 430, p. 339–348, https://doi.org/10.1016/j.epsl.2015.08.008

Millot, R., Gaillardet, J., Dupre, B., and Allegre, C. J., 2003, Northern latitude chemical weathering rates: Clues from the Mackenzie River Basin, Canada: Geochimica et Cosmochimica Acta, v. 67, n. 7, p. 1305–1329, https://doi.org/10.1016/S0016-7037(02)01207-3

Moon, S., Chamberlain, C. P., and Hilley, G. E., 2014, New estimates of silicate weathering rates and their uncertainties in global rivers: Geochimica et Cosmochimica Acta, v. 134, p. 257–274, https://doi.org/10.1016/j.gca.2014.02.033

Pagani, M., Caldeira, K., Berner, R., and Beerling, D. J., 2009, The role of terrestrial plants in limiting atmospheric $CO_2$ decline over the past 24 million years: Nature, v. 460, p. 85–88, https://doi.org/10.1038/nature08133

Pearson, D. G., Irvine, G. J., Ionov, D. A., Boyd, F. R., and Dreibus, G. E., 2004, Re-Os isotope systematics and platinum group element fractionation during mantle melt extraction: A study of massif and xenolith peridotite suites: Chemical Geology, v. 208, n. 1–4, p. 29–59, https://doi.org/10.1016/j.chemgeo.2004.04.005

Petsch, S. T., 2014, Weathering of organic carbon: Treatise on Geochemistry, Second Edition, v. 12, p. 217–238, https://doi.org/10.1016/B978-0-08-095975-7.01013-5

Petsch, S. T., Berner, R. A., and Eglinton, T. I., 2000, A field study of the chemical weathering of ancient sedimentary organic matter: Organic Geochemsitry, v. 31, n. 5, p. 475–487, https://doi.org/10.1016/S0146-6380(00)00014-0

Rahaman, W., Singh, S. K., and Shukla, A. D., 2012, Rhenium in Indian rivers: Sources, fluxes, and contribution to oceanic budget: Geochemistry, Geophysics, Geosystems, v. 13, n. 8, https://doi.org/10.1029/2012GC004083

Reeder, S. W., Hitchon, B., and Levinson, A. A., 1972, Hydrogeochemistry of the surface waters of the Mackenzie River drainage basin, Canada—I. Factors controlling inorganic composition: Geochimica et Cosmochimica Acta, v. 36, n. 8, p. 825–865, https://doi.org/10.1016/0016-7037(72)90053-1

Reimer, P. J., Brown, T. A., and Reimer, R. W., 2004, Discussion: Reporting and calibration of post-bomb ^{14}C data: Radiocarbon, v. 46, n. 3, p. 1299–1304, https://doi.org/10.1017/S0033822200033154

Reisberg, L., and Lorand, J. P., 1995, Longevity of sub-continental mantle lithosphere from osmium isotope

systematics in orogenic peridotite massifs: Nature, v. 376, p. 159–162, https://doi.org/10.1038/376159a0

Ross, D. J. K., and Bustin, R. M., 2009, Investigating the use of sedimentary geochemical proxies for paleoenvironment interpretation of thermally mature organic-rich strata: Examples from the Devonian-Mississippian shales, Western Canadian Sedimentary Basin: Chemical Geology, v. 260, n. 1–2, p. 1–19, https://doi.org/10.1016/j.chemgeo.2008.10.027

Selby, D., and Creaser, R. A., 2003, Re-Os geochronology of organic rich sediments: An evaluation of organic matter analysis methods: Chemical Geology, v. 200, n. 3–4, p. 225–240, https://doi.org/10.1016/S0009-2541(03)00199-2

Soulet, G., Hilton, R. G., Garnett, M. H., Dellinger, M., Croissant, T., Ogrič, M., and Klotz, S., 2018, Technical note: *In situ* measurement of $CO_2$ released during weathering of rocks: Biogeosciences, v. 15, n. 13, p. 4087–4102, https://doi.org/10.5194/bg-15-4087-2018

Tank, S. E., Frey, K. E., Striegl, R. G., Raymond, P. A., Holmes, R. M., McClelland, J. W., and Peterson, B. J., 2012, Landscape–level controls on dissolved carbon flux from diverse catchments of the circumboreal: Global Biogeochemical Cycles, v. 26, n. 4, https://doi.org/10.1029/2012GB004299

Tank, S. E., Striegl, R. G., McClelland, J. W., and Kokelj, S. V., 2016, Multi-decadal increases in dissolved organic carbon and alkalinity flux from the Mackenzie drainage basin to the Arctic Ocean: Environmental Research Letters, v. 11, n. 5, https://doi.org/10.1088/1748-9326/11/5/054015

Tipper, E. T., Bickle, M. J., Galy, A., West, A. J., Pomiès, C., and Chapman, H. J., 2006, The short term climatic sensitivity of carbonate and silicate weathering fluxes: Insight from seasonal variations in river chemistry: Geochimica et Cosmochimica Acta, v. 70, n. 11. p. 2737–2754, https://doi.org/10.1016/j.gca.2006.03.005

Torres, M. A., West, A. J., and Li, G., 2014, Sulphide oxidation and carbonate dissolution as a source of $CO_2$ over geological timescales: Nature, v. 507, p. 346–349, https://doi.org/10.1038/nature13030

Torres, M. A., West, A. J., Clark, K. E., Paris, G., Bouchez, J., Ponton, C., Feakins, S. J., Galy, V., and Adkins, J. F., 2016, The acid and alkalinity budgets of weathering in the Andes–Amazon system: Insights into the erosional control of global biogeochemical cycles: Earth and Planetary Science Letters, v. 450, p. 381–391, https://doi.org/10.1016/j.epsl.2016.06.012

Torres, M. A., Moosdorf, N., Hartmann, J., Adkins, J. F., and West, A. J., 2017, Glacial weathering, sulfide oxidation, and global carbon cycle feedbacks: Proceedings of the National Academy of Sciences of the United States of America, v. 114, n. 33, p. 8716–8721, https://doi.org/10.1073/pnas.1702953114

Turchyn, A. V., Tipper, E. T., Galy, A., Lo, J .K., and Bickle, M. J., 2013, Isotope evidence for secondary sulfide precipitation along the Marsyandi River, Nepal, Himalayas: Earth and Planetary Science Letters, v. 374, p. 36–46, https://doi.org/10.1016/j.epsl.2013.04.033

Vonk, J. E., Giosan, L., Blusztajn, J., Montlucon, D., Pannatier, E. G., McIntyre, C., Wacker, L., Macdonald, R. W., Yunker, M. B., and Eglinton, T. I., 2015, Spatial variations in geochemical characteristics of the modern Mackenzie Delta sedimentary system: Geochimica et Cosmochimica Acta, v. 171, p. 100–120, https://doi.org/10.1016/j.gca.2015.08.005

von Strandmann, P. A. E. P., Burton, K. W., James, R. H., van Calsteren, P., Gislason, S. R., and Sigfússon, B., 2008, The influence of weathering processes on riverine magnesium isotopes in a basaltic terrain: Earth and Planetary Science Letters, v. 276, n. 1–2, p. 187–197, https://doi.org/10.1016/j.epsl.2008.09.020

West, A. J., Galy, A., and Bickle, M., 2005, Tectonic and climatic controls on silicate weathering: Earth and Planetary Science Letters, v. 235, n. 1–2, p. 211–228, https://doi.org/10.1016/j.epsl.2005.03.020

Wheeler, J. O., Hoffman, P. F., Card, K. D., Davidson, A., Sanford, B. V., Okulitch, A. V., and Roest, W. R., 1996, Geological map of Canada: Natural Resources Canada, "A" Series Map 1860A, 3 sheets, 1:5,000,000, https://doi.org/10.4095/208175

White, A. F., and Brantley, S. L., 2003, The effect of time on the weathering of silicate minerals: Why do weathering rates differ in the laboratory and field?: Chemical Geology, v. 202, n. 3–4, p. 479–506, https://doi.org/10.1016/j.chemgeo.2003.03.001

Winnick, M. J., Carroll, R. W. H., Williams, K. H., Maxwell, R. M., Dong, W., and Maher, K., 2017, Snowmelt controls on concentration-discharge relationships and the balance of oxidative and acid-base weathering fluxes in an alpine catchment, East River, Colorado: Water Resources Research, v. 53, n. 3, https://doi.org/10.1002/2016WR019724

Yeghicheyan, D., Bossy, C., Bouhnik Le Coz, M., Douchet, C., Granier, G., Heimburger, A., Lacan, F., Lanzanova, A., Rousseau, T. C. C., Seidel, J.-L., Tharaud, M., Candaudap, F., Chmeleff, J., Cloquet, C., Delpoux, S., Labatut, M., Losno, R., Pradoux, C., Sivry, Y., and Sonke, J. E., 2013, A Compilation of Silicon, Rare Earth Element and Twenty-One other Trace Element Concentrations in the Natural River Water Reference Material SLRS-5 (NRC-CNRC): Geostandards and Geoanalytical Research, v. 37, n. 4, p. 449–467, https://doi.org/10.1111/j.1751-908X.2013.00232.x